Molecular signatures and associated regulators of the pea leaf response to sulfur deficiency and water deficit as revealed by multi-omics analyses

Titouan Bonnot[1], Charlotte Henriet[1], Delphine Aimé[1], Jonathan Kreplak[1], Morgane Térézol[1§], Thierry Balliau[2], Alain Ourry[3], Michel Zivy[2], Vanessa Vernoud[1,*] and Karine Gallardo[1,*]

[1] Agroécologie, INRAE, Institut Agro, Univ. Bourgogne, Univ. Bourgogne Franche-Comté, F-21000 Dijon, France

[2] Plateforme d'Analyse de Protéomique Paris Sud-Ouest (PAPPSO), Université Paris-Saclay, INRAE, CNRS, AgroParisTech, UMR Génétique Quantitative et Évolution-Le Moulon, 91190 Gif-sur-Yvette, France

[3] UMR 950 Ecophysiologie Végétale, Agronomie et Nutritions N, C, S, Normandie Université, UNICAEN, INRAE, Caen, France

[§] Present address: Aix Marseille Univ, INSERM, MMG, Marseille, France

* These authors contributed equally

Corresponding author: titouan.bonnot@inrae.fr

Abstract

Sulfur availability in soils affects both yield and seed quality in major crops, and the plant capacity to tolerate environmental constraints. Under stress combination, plants often show specific responses at the molecular level. To dissect the molecular responses to sulfur deficiency in interaction or not with water deficit, a multi-omics approach was used focusing on the leaves of pea (*Pisum sativum*), at several days during the early reproductive phase. Using ionomics, transcriptomics, proteomics and gene network analyses, we identified a module of genes strongly driven by sulfur availability. This includes known and putative new players of plant responses to sulfur-deprived conditions. Conserved profiles between proteins and mRNAs were specifically observed within this module, suggesting transcriptional regulation. While moderate water deficit had little impact when occurring alone, it thoroughly perturbed plant growth and the leaf transcriptome and proteome when combined with sulfur deficiency. Under this stress combination, molecular responses were amplified, notably at the transcriptome level, in a time-specific manner. Genes with specific or

35 greater responses under this condition were identified, and transcriptional regulators
36 of the highlighted genes and pathways were predicted, which may represent
37 interesting targets to develop crops tolerant to multi-stress conditions.
38
39 **Introduction**
40 Human activities are responsible for global changes such as global warming and
41 climate change, some of which are now inevitable and irreversible (IPCC 2023).
42 Besides an increase in both the intensity and frequency of extreme events, the number
43 of factors and their interactions, that affect ecosystem functioning, are growing rapidly
44 (Paine et al. 1998; IPCC 2023). In the field, plants can face multiple growth-limiting
45 stresses that can occur sequentially or simultaneously, such as elevated temperatures
46 and water deficit (WD), or WD and nutrient deficiencies (Mittler 2006; Lecomte et al.
47 2023). Combination of stresses can have a more dramatic impact on crop yields than
48 individual stress conditions, as observed under combined heat stress and drought or
49 under drought and sulfur (S) deficiency (Henriet et al. 2019; Cohen et al. 2021). At the
50 molecular level, previous studies performed in controlled or semi-controlled conditions
51 revealed that combination of stresses often resulted in unique molecular signatures,
52 that could not be predicted by studying the plant responses to each individual stress
53 (Rizhsky et al. 2002, 2004; Mittler 2006; Rasmussen et al. 2013; Zandalinas et al.
54 2021; Mahalingam et al. 2022; Tan et al. 2023). For example, ~55% of genes
55 responding to heat and/or drought stress in Arabidopsis showed antagonistic or
56 synergistic responses under combined heat stress and drought (Azodi et al. 2020).
57 Such specificities may reflect the activation of unique biological pathways that are
58 critical for the plant tolerance to a given combination of stresses (Zandalinas et al.
59 2021), and need to be considered for improving the tolerance to environmental
60 constraints. While extensive work has been done to study plant responses to a wide
61 variety of single stress treatments, little is still known about responses to multi-stress
62 conditions in crops, especially at the molecular level (Zandalinas and Mittler 2022).
63 To limit global warming to the most optimistic scenarios, deep and rapid cuts in
64 greenhouse gas emissions are needed (IPCC 2023). Increasing the cultivation of
65 pulses – which generates little CO_2 as compared to the production of other major foods
66 (Poore and Nemecek 2018) – would contribute to this effort. Moreover, the capacity of
67 legume species to fix atmospheric N_2 through root nodule symbiosis allows them to
68 accumulate high amounts of proteins in seeds without the need of nitrogen (N)

fertilization, which makes them interesting protein-rich alternatives to animal-based foods (Stagnari et al. 2017; Detzel et al. 2022). Although recent advances in the development of genomic tools and technologies have allowed an acceleration of breeding programs in legumes (Varshney et al. 2019), environmental constraints such as abiotic stresses represent major limiting factors for yield potential in species such as pea (*Pisum sativum* L.; Lecomte et al. 2023). A better understanding of the molecular responses of pulses to multi-stress conditions is therefore needed.

Sulfur starvation in soils is reported worldwide, due to several factors such as stricter regulations on industrial SO_2 emissions and the declining use of S-containing pesticides and S fertilizers. This results in S deficiency symptoms in crops, and affects both yield and seed quality (Scherer 2001; Haneklaus et al. 2008; Poisson et al. 2019; Borja Reis et al. 2021). In pea seeds, but also in cereals like wheat, the balance between S and N strongly influences storage protein composition, a key determinant of seed quality (reviewed in Mondal et al. 2022; Bonnot et al. 2023). Previous work in Arabidopsis has revealed genes that are activated under S-deficient conditions, including a set of genes co-expressed with O-acetylserine (OAS) accumulation, known as the OAS cluster genes (Hubberten et al. 2012; Aarabi et al. 2016, 2021). Several members of the OAS cluster are also induced in wheat and pea seeds under S-deficient conditions (Bonnot et al. 2020; Henriet et al. 2021). Some studies suggest a role of this cluster in S sensing and signaling (Ristova and Kopriva 2022). Since S is essential for the synthesis of several antioxidant molecules like glutathione, S- also alters the plant capacity to cope with other environmental constraints (Samanta et al. 2020). However, connections between known regulatory genes of the plant response to S-limiting conditions and of pathways of response to abiotic stresses are still unclear.

We previously investigated the interaction between S- and WD during the early reproductive phase in pea (Henriet et al. 2019, 2021), and showed that the combination of the stresses negatively impacted seed yield and seed size in a synergistic manner (Henriet et al. 2019). However, WD mitigated the impact of S- on the seed storage protein composition, suggesting that under stress combination, pea plants employed a strategy to produce fewer seeds with a well-balanced protein composition (Henriet et al. 2019, 2021). At the molecular level, fewer transcripts and proteins were differentially accumulated in developing seeds when the two stresses were combined, as compared to S-. In fact, the response of developing pea seeds to S- in combination with WD depends on a small number of proteins with important protective functions against

oxidative damage or in repair processes. This led us to speculate that most molecular responses activated under combined WD and S- may have occurred in other tissues, in particular in leaves that are a rich source of nutrients for the developing seeds.

To further dissect the molecular pathways activated under WD and S-, we used a multi-omics approach focusing on pea leaves. Transcriptomics, proteomics and ionomics data were obtained at different time points during stresses applied individually or in combination, on leaf samples collected from the experiment described in Henriet et al. (2019, 2021). A highly specific module of genes responding to S- (occurring alone or in combination with WD) was revealed, with known and putative new regulators of the plant's responses to this stress. Our results also emphasized that combination of S- and WD induced specific or amplified responses as compared to single stress conditions. Besides a critical impact on the plant phenotype, the combined stress thoroughly perturbed the leaf transcriptome, proteome and ionome. The transcriptome remarkably responded to this condition, in a time-specific manner. Network analyses allowed us to identify molecular signatures that are specific to this condition and to predict potential regulatory genes of selected modules.

Results

Water deficit combined with S deficiency severely affects the plant growth

To explore the interplay between WD and S-, plants were exposed to either S- starting three weeks after sowing (5/6 leaf stage), moderate WD (50% of the water holding capacity of the substrate) applied at the beginning of flowering for nine days, or to the combination of WD and S- (WD/S-, Figure 1A). The S- treatment was applied 16 days before WD, to ensure that leaf S content was perturbed before water stress imposition. The experimental setup is detailed in (Henriet et al. 2019, 2021). Phenotypic variables were measured in different plant compartments, and leaves of the first two reproductive nodes were collected from control and stressed plants at days 0 (for control and S- conditions only), 2, 5, 9 and 12 to conduct -omics analyses (Figure 1; Supplemental Data Set S1). For conditions WD and WD/S-, day 12 corresponds to three days of rewatering, and informs on the plant recovery after WD. Separate statistical analyses were performed for data obtained at day 0 and day 12 due to different treatment modalities compared to the other time points (see methods). Few effects of WD applied alone on the measured traits were observed (Figure 1B; Supplemental Data Set S2). The only significant changes were a decrease in the dry weight of leaves from the

reproductive part of the plant at day 12 (Figure 1B; Supplemental Data Set S1), and a lower osmotic potential at day 5 (-1.34 MPa under WD, -1.21 MPa under control conditions, $P \approx$ 2.8E-03; Figure 1C; Supplemental Data Sets S1 and S2).

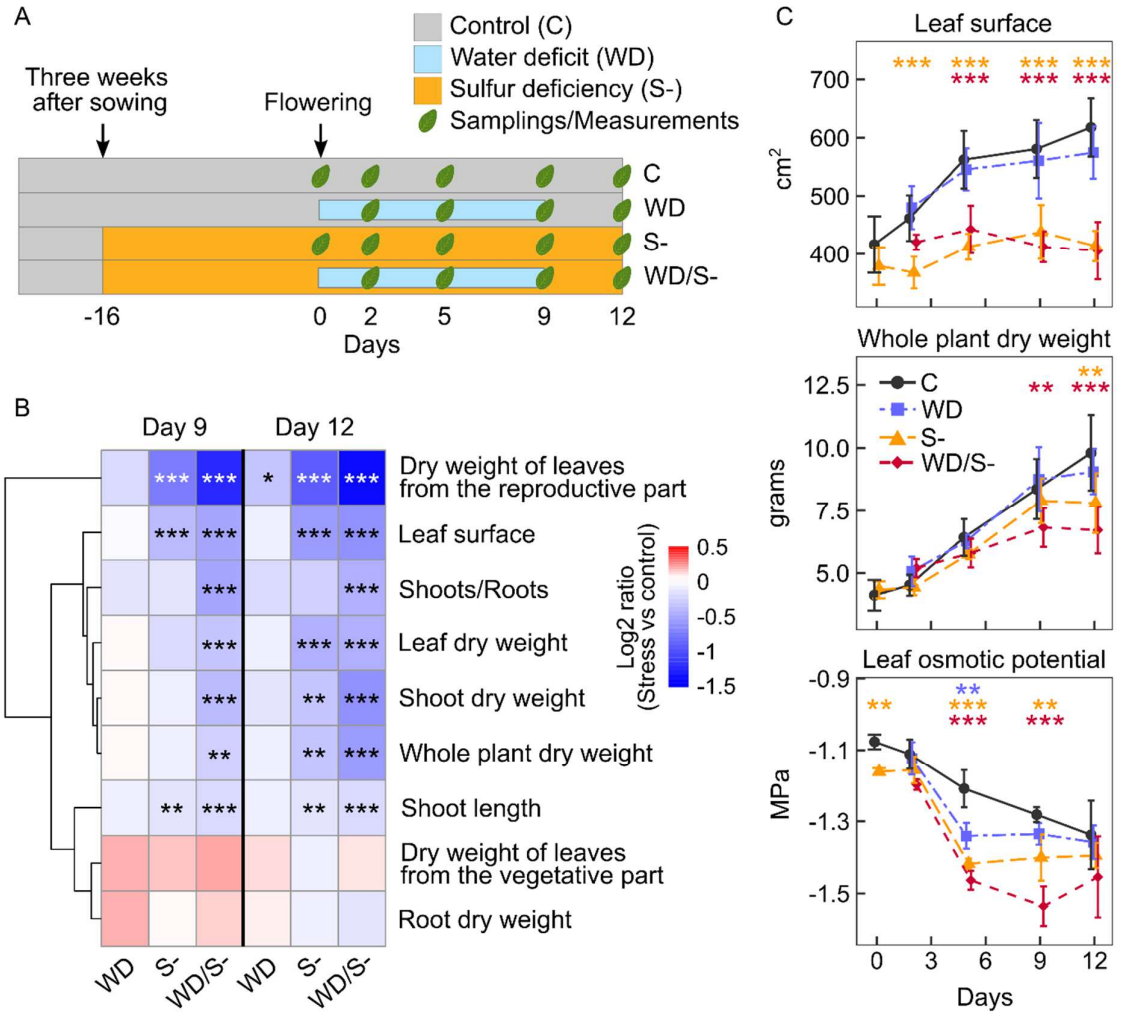

Figure 1. Influence of water deficit (WD), sulfur deficiency (S-) and combined stresses on pea plant phenotypic variables. A, Experimental design. Days 0 and 9 correspond to the beginning and end of WD, respectively. For the conditions WD and WD/S-, day 12 corresponds to three days of rewatering for plant recovery. B, Effects of stresses on phenotypic variables, at the end of the WD stress imposition (day 9) and after three days of rewatering (day 12). Data are represented as heatmaps, blue and red representing lower and higher values in the stress condition as compared to control, respectively. Variables with similar responses to stress are grouped using a hierarchical clustering method. Data are means ± S.D. of $n = 8$ biological replicates (eight individual plants per condition). Raw data are presented in Supplemental Data Set S1. C, Profile of leaf surface, whole plant dry weight and leaf osmotic potential. Data are means ± S.D. of $n = 8$ (surface and weight) or n=4 (osmotic potential) biological replicates. In B and C, asterisks indicate significant differences between stress and control conditions (*, $P < 0.05$; **, $P < 0.01$; ***, $P < 0.001$). In C, orange, blue and red asterisks refer to S-, WD and WD/S- conditions, respectively. Three separate statistical analyses were performed: comparison of S- and control at day 0 (Student's t-test); comparisons of all treatments from day 2 to day 9 (two-way ANOVA); comparisons of all treatments at day 12 during the plant recovery (one-way ANOVA, see methods for details).

158 Under S-, several plant traits were affected, with a significant reduction in leaf
159 surface, shoot length, and in leaf, shoot and whole plant dry weight (Figure 1, B and
160 C; Supplemental Data Set S2). Together with a significant reduction in the leaf osmotic
161 potential (days 0, 5 and 9), these results highlighted the negative impact of S- on the
162 plant development and physiology (Figure 1C; Supplemental Data Set S2). Of note,
163 the significant reduction of the leaf osmotic potential at day 0 under S- indicates that
164 our S deficiency treatment induced a stress before the WD imposition.
165 When the two stresses were combined (WD/S-), the plant height, the leaf surface
166 area, the plant biomass and the shoot-to-root ratio were strongly affected (Figure 1, B
167 and C). This was observed at both day 9, when stress intensity was the highest, and
168 at day 12, *i.e.* three days after plant rewatering (Figure 1B). For example, at day 12,
169 the leaf surface area and the whole plant dry weight were reduced by 34.3% ($P \approx$
170 6.14E-09) and by 31.5% ($P \approx$ 6.14E-05), respectively (Figure 1, B and C; Supplemental
171 Data Sets S1 and S2). Measurements of the leaf osmotic potential confirmed the
172 amplified effect induced by the stress combination, with the lowest osmotic potential
173 value measured at day 9 under WD/S- (-1.54 MPa, Figure 1C; Supplemental Data Set
174 S1). Taken together, these results showed that while the WD treatment had moderate
175 effects compared to S-, it severely affected plant growth when combined with S-.
176

177 **Nutrients and potentially toxic elements show specific accumulation profiles in**
178 **response to single and combined stress treatments**

179 To estimate the impact of the single or combined stresses on the plant nutritional
180 status, we next quantified the carbon (C), N and S contents in leaves using the Dumas
181 method (Supplemental Data Set S1). No significant differences were observed in
182 response to WD applied alone, although leaf N content tends to be lower under this
183 condition (Figure 2A). Both S- and WD/S- treatments significantly reduced leaf C, N
184 and S contents at one or more time points (Figure 2A; Supplemental Data Set S2). At
185 day 0, all three elements were significantly less accumulated in response to S- (Figure
186 2A), indicating that the leaf elemental composition was altered even before WD
187 imposition, as expected from our experimental design where S- was applied at the 5/6
188 leaf stage, *i.e.* about 16 days before the onset of WD. S-deficient treatments (S- and
189 WD/S-) remarkably impacted S content in leaves, which dropped from 0.23% of the
190 leaf dry weight (on average, from day 2 to day 12) in control condition to 0.090% and
191 0.087% in response to S- and WD/S-, respectively (Figure 2A; Supplemental Data Set

192 S1). With no clear distinction between control and WD, or between S- and WD/S-, this
193 highlights that our S- treatment strongly reduced S accumulation and/or transport in
194 pea leaves, regardless of water supply. Changes in C, N and S contents under stress
195 therefore altered the balance between these elements in leaves, especially the N/S
196 ratio, which highly increased under both S- and WD/S- (Figure 2A).

197 To further evaluate the perturbations induced by stresses on the plant nutrition, we
198 extended our analyses to other essential macro-nutrients (phosphorus, potassium,
199 calcium, magnesium), micro-nutrients (iron, boron, manganese, zinc, copper,
200 molybdenum, nickel) and other elements (cobalt, cadmium, lead, arsenic, vanadium)
201 using high-resolution inductively coupled plasma mass spectrometry (HR ICP-MS,
202 Figure 2B; Supplemental Data Set S1; Supplemental Figure S2). This analysis also
203 included the quantification of S, which showed very consistent results as those
204 obtained with the Dumas method (R = 0.9; Supplemental Figure S1). Molybdenum
205 showed remarkable higher contents in leaves under S- and WD/S- as compared to
206 control and WD conditions at all time points, and was strongly correlated with S content
207 (R = -0.78) and N/S ratio (R = 0.85) variables (Figure 2, B and C).

208 All macro- and micro-nutrients, except molybdenum and nickel, were less
209 accumulated in leaves under S- as compared to control (Figure 2B; Supplemental
210 Figure S2), suggesting that S deprivation altered the uptake and transport of other
211 nutrients in leaves, as previously reported in pea (Jacques et al. 2021). Significant
212 reduced accumulation of S in leaves was also observed under WD at day 2 (Figure
213 2B; Supplemental Figure S2; Supplemental Data Set S2). In response to WD,
214 accumulation of iron, magnesium and zinc in leaves tended to increase, and this
215 increase was even more pronounced when plants were exposed to WD/S-, especially
216 from days 5 to 12 (Figure 2B; Supplemental Figure S2). While iron and zinc are two
217 essential micro-nutrients, they become toxic at high concentration (Connolly and
218 Guerinot 2002; Balafrej et al. 2020). Similarly, hyperaccumulation of cobalt, specifically
219 observed at day 9 under WD/S- and during recovery at day 12 (Figure 2B;
220 Supplemental Figure S2), can be detrimental to plants (Hu et al. 2021). Non-essential
221 elements that can cause deleterious effects on plant growth, such as arsenic and
222 cadmium, were also more accumulated in response to WD/S- (Figure 2B;
223 Supplemental Figure S2). Increased accumulation of cadmium in leaves was also
224 detected in response to S-, specifically from day 0 to day 5 (Supplemental Figure S2).

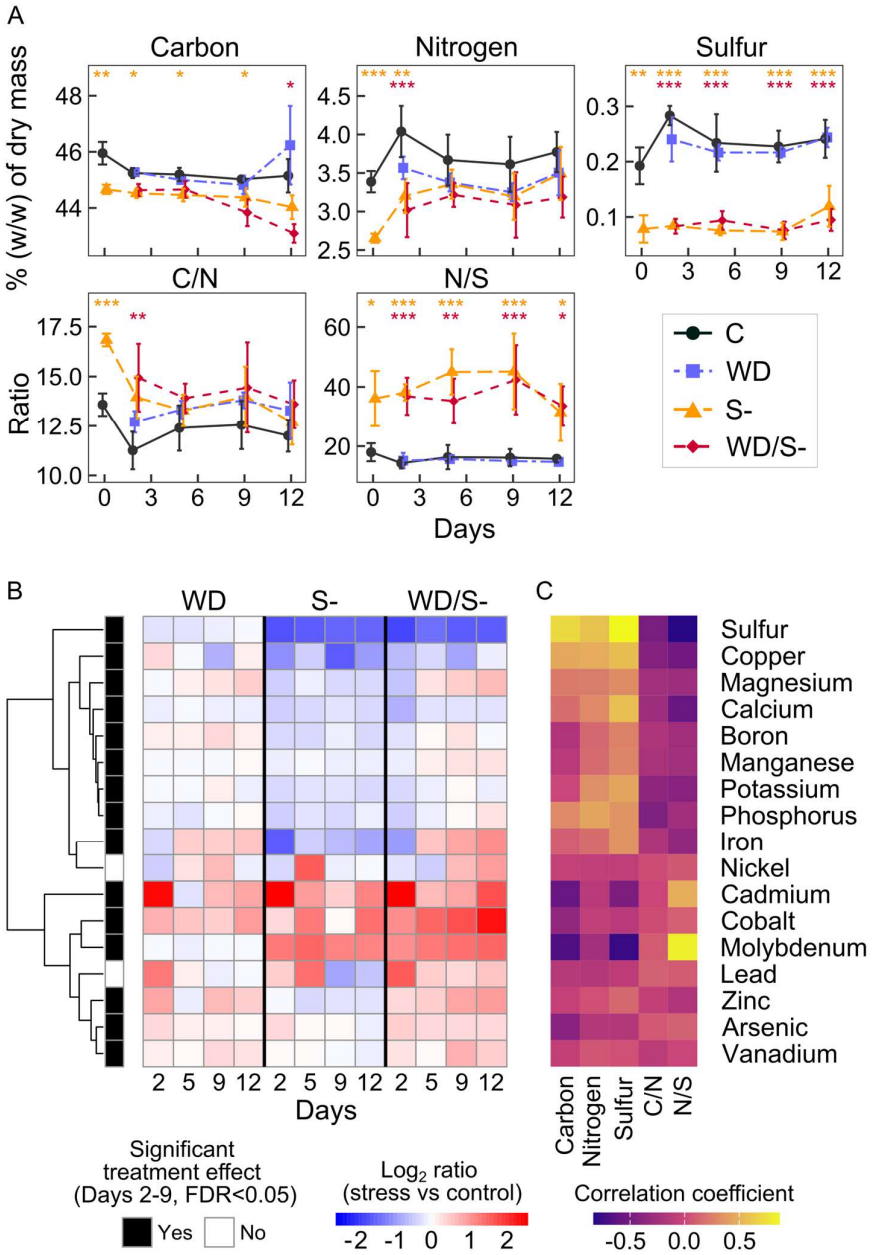

Figure 2. Elemental composition of elements in pea leaves in response to water deficit (WD), sulfur deficiency (S-) and combined stress. A, Profiles of accumulation of Carbon (C), Nitrogen (N), Sulfur (S), as well as C/N and N/S ratios (means ± S.D, *n* = 4 biological replicates). Asterisks indicate significant differences between stress and control conditions (*, P < 0.05; **, P < 0.01; ***, P < 0.001). Orange and red asterisks refer to S- and WD/S- conditions, respectively. Three separate statistical analyses were performed: comparison of S- and control at day 0 (Student's t-test); comparisons of all treatments from day 2 to day 9 (two-way ANOVA); comparisons of all treatments at day 12 during the plant recovery (one-way ANOVA, see methods for details). B, Heatmap representing the change in leaf dry matter content of elements in response to stresses. Blue and red colors represent lower and higher values in the stress condition as compared to control, respectively. Elements with similar profiles are grouped using a hierarchical clustering method. Elements with a significant treatment effect (FDR < 0.05, ANOVA) during the period from day 2 to day 9 are highlighted with a black square. Raw data are provided in Supplemental Data Set S1 and statistical results (including comparison of treatments at day 12) are in Supplemental Data Set S2. C, Heatmap of Spearman correlation between element content and variables presented in A. Yellow and purple colors represent positive and negative correlation coefficients, respectively.

242 Taken together, these results showed that stress treatments, especially when
243 combined, led to the accumulation of elements which can compromise plant growth
244 and survival. Zinc, iron and cobalt were particularly accumulated in leaves under
245 WD/S- and therefore represent markers of the combined stress condition, whereas S
246 content, N/S and molybdenum are more specific indicators of S- combined or not with
247 WD.
248
249 **Stress combination thoroughly perturbs the leaf transcriptome and proteome**
250 To identify genes and biological pathways that are regulated under WD and/or S- and
251 that could be important for the plant tolerance to these stresses, we explored the
252 responses at the transcriptome and proteome levels, using RNA-Sequencing and
253 shotgun proteomics, respectively. In total, 29572 genes were considered as expressed
254 in the experiment (see Methods) and 2261 proteins were successfully quantified
255 (Figure 3A; Supplemental Data Set S3). Since day 12 corresponds to the recovery
256 period after WD, omics data obtained at this time point were statistically analyzed
257 separately (Figure 3A, see Methods).
258 First, analyses of variance at days 2-9 revealed that the treatments significantly
259 (FDR < 0.05) altered the expression of 14497 (49%) genes and the accumulation of
260 1327 (58.7%) proteins (Figure 3A; Supplemental Data Set S2). The analysis from days
261 2-9 also highlighted that 33.6% of the transcriptome showed a significant time ×
262 treatment interaction effect, meaning that responses to treatments are influenced by
263 time for these genes (Figure 3A). This proportion was much lower at the proteome
264 level (3.4%), suggesting smaller variations in the stress response over time for
265 proteins. We therefore asked to what extent effects of the stresses on the
266 transcriptome were conserved at the protein level. To this aim, we compared the
267 protein and mRNA profiles of the 2240 genes analyzed in both datasets (Supplemental
268 Data Set S4). Considering the whole datasets (all treatments combined, day 2 to day
269 12), correlations between mRNAs and proteins ranged from -0.67 to 0.92, with a
270 median at 0.12 (Figure 3B). This overall low correlation indicates that post-
271 transcriptional regulations may strongly influence mRNA translation for a large
272 proportion of the 2240 genes. A similar analysis performed for each treatment showed
273 comparable trends, excluding a potential effect of stresses on the overall correlation
274 between mRNA and protein profiles (Figure 3C). Nonetheless, we identified a group of
275 308 genes (13.7%) with a correlation greater than 0.5, which are involved in the

biosynthesis of S-containing molecules (Met, Cys, glutathione), and in the response to various stresses including cadmium and oxidative stress (Figure 3, B and D; Supplemental Data Sets S4 and S5). These genes exhibiting higher correlations between their mRNA and protein profiles may be more strongly regulated at the transcriptional level than at the post-transcriptional level.

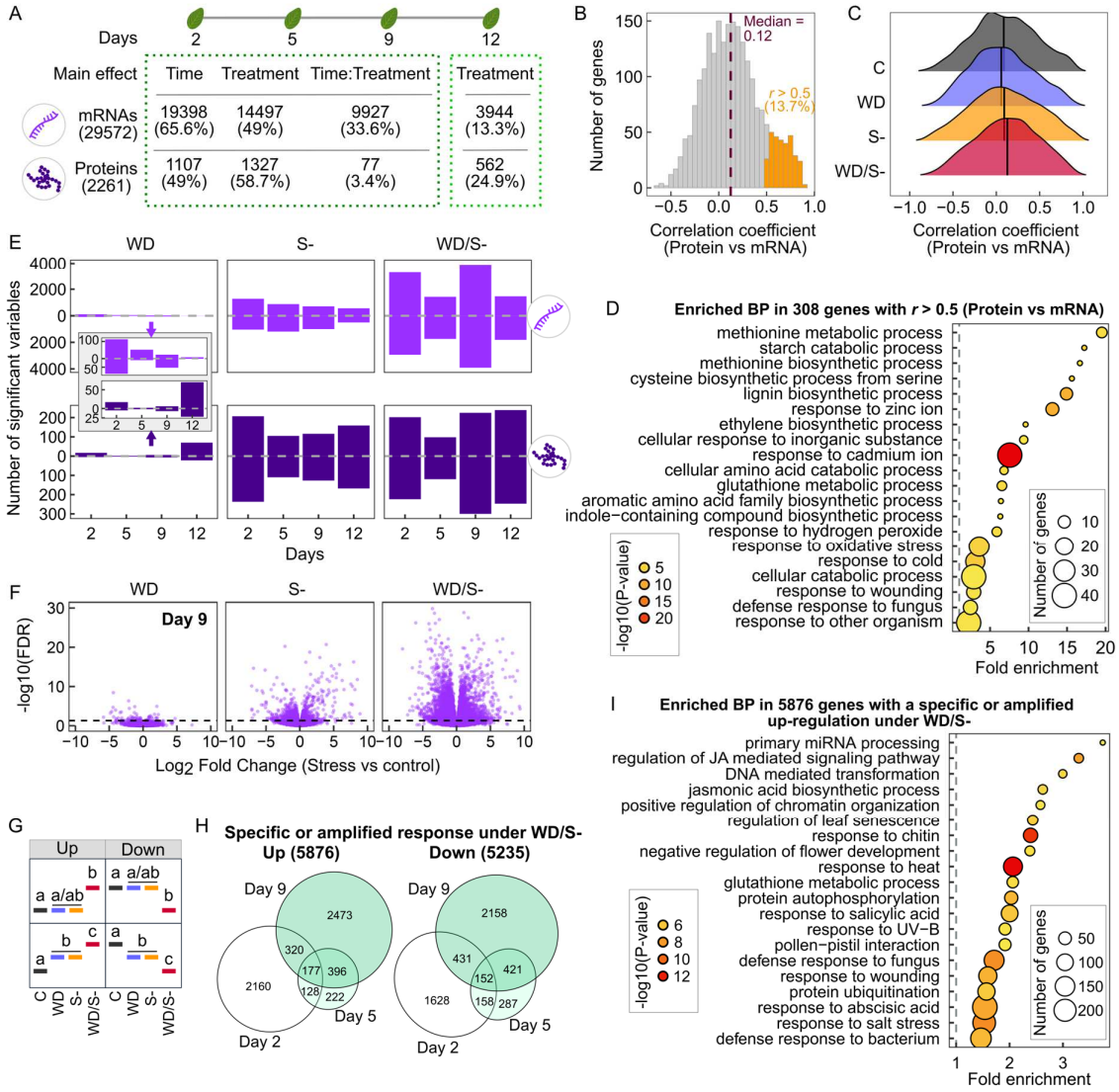

Figure 3. Transcriptome and proteome responses to stress reveal genes with specific or amplified responses under combined stress condition. A, Results of statistical analyses showing the number of mRNAs and proteins with a significant (FDR < 0.05) effect of time, treatment, and the interaction between time and treatment (Time:Treatment). Two separate analyses were performed, one for day 2 to day 9, for which conditions were the same (Two-way ANOVA), and one for day 12, during the plant recovery following WD (One-way ANOVA). The percentage of analyzed molecules with a significant effect is indicated in parentheses (*e.g.* the accumulation of 49% of the proteome is significantly affected by time). B, Histogram showing the distribution of correlation (Spearman) coefficients for the comparisons between proteins and mRNAs (data obtained at days 2, 5, 9 and 12 from all treatment conditions). Genes with a $r > 0.5$ (protein vs mRNA) are highlighted in orange. C, Ridgeline plots showing

293 the distribution of correlation (Spearman) coefficients for the comparison between proteins and mRNAs,
294 for each condition (conditions were separated for the calculation of correlation coefficients). Vertical
295 black lines indicate medians. In total, 2240 genes were analyzed at both transcriptomic and proteomic
296 levels, and were therefore considered for the analyses shown in B and C. D, Selected enriched biological
297 processes in genes with a $r > 0.5$ (protein vs mRNA) identified in B. The top 20 enriched GO terms
298 (based on P-values) with at least five genes are represented. E, Barplots showing the numbers of
299 differentially accumulated mRNAs and proteins in response to the stress conditions as compared to
300 control, at each developmental stage. This results from pairwise comparisons following the analysis
301 presented in A (variables with a significant treatment effect were used for pairwise comparisons). For
302 WD, zoomed plots are shown to reveal differences between time points. F, Volcano plots representing
303 statistical significance (-log10[FDR]) versus magnitude of change (Log_2 Fold Change) for mRNAs at
304 Day 9. G, Schematic plot summarizing situations where mRNAs were considered as having a specific
305 or amplified response in the combined stress as compared to single stress conditions. H, Venn diagrams
306 depicting the overlap between lists of genes identified at days 2, 5 and 9 with a specific or amplified
307 response in the combined stress condition. I, Selected enriched biological processes in genes with a
308 specific or amplified up-regulation under WD/S- as compared to single stress conditions. The top 20
309 enriched GO terms (based on P-values) are represented.

310

311 Second, pairwise comparisons performed on variables with a significant treatment
312 effect (FDR < 0.05) revealed that many more mRNAs and proteins were differentially
313 accumulated in response to S- and WD/S- than to WD applied alone (Figure 3E;
314 Supplemental Data Set S2). The number of differentially accumulated molecules also
315 differed depending on the days (Figure 3E). For instance, under WD/S-, 3286, 1430
316 and 3901 genes and 202, 98 and 225 proteins were up-regulated at days 2, 5 and 9,
317 respectively (Figure 3E). Thus, more than twice less genes and proteins were up-
318 regulated at day 5 under WD/S- compared to day 2 or day 9. The influence of time is
319 stronger under WD and WD/S- than under S-, which could be explained by our
320 experimental design, where S deficiency was applied earlier in the plant development
321 as compared to WD (Figure 1A). The transcriptome and proteome reprogramming at
322 day 9 was specifically observed under WD/S-, and may be associated with an intense
323 stress response. Indeed, we observed that S-deficient plants did not survive to a
324 prolonged period of WD (leaves of plants experiencing 12 days of combined stress
325 dried out, Henriet et al., 2019).

326 Third, we observed that numbers of differentially expressed genes (DEGs) and, to
327 a lesser extent, of differentially accumulated proteins, were larger under WD/S- than
328 under single stresses (Figure 3E). At the transcriptome level, both lower P-values and
329 higher fold change values were observed under this condition (Figure 3F;
330 Supplemental Figure S3). For instance, at day 9, 3901 up-regulated DEGs were
331 identified under WD/S-, whereas only 23 and 709 genes were up-regulated in response
332 to WD and S-, respectively (Figure 3E). To explore this greater response under stress
333 combination, we isolated genes between day 2 and day 9 with either 1) a specific

334 response under WD/S- (and not under WD or S-, upper panel, Figure 3G), or 2) a
335 greater response under WD/S- as compared to single stress conditions (lower panel,
336 Figure 3G). In total, we identified 5876 up-regulated and 5235 down-regulated DEGs
337 with a specific or amplified response under WD/S- (Figure 3H; Supplemental Data Set
338 S6). The up-regulated DEGs were enriched in genes involved in the response to
339 diverse stresses (*e.g.* heat, UV-B, salt, wounding, fungus), in the response or
340 biosynthesis of hormones (jasmonic acid, salicylic acid, abscisic acid), in epigenetic-
341 related processes (primary miRNA processing, positive regulation of chromatin
342 organization), in glutathione metabolic process and protein modification
343 (autophosphorylation, ubiquitination; Figure 3I; Supplemental Data Set S5). On the
344 contrary, down-regulated DEGs have a role in photosynthesis, photorespiration,
345 phototropism and gravitropism, as well as in translation or response to cold
346 (Supplemental Figure S4, Supplemental Data Set S5). Interestingly, the lists of DEGs
347 with a specific or amplified response were very different depending on the day, with for
348 example 2160 (37%) and 2473 (42%) of the up-regulated DEGs that were specific to
349 day 2 and day 9, respectively (Figure 3H). This result shows that a sequential response
350 is observed under WD/S-, with two waves of response involving different sets of genes.
351

352 **Co-expression network analysis identifies treatment-driven modules with**
353 **contrasted patterns of response**

354 To further investigate the influence of treatments on gene expression in leaves and to
355 identify genes with specific patterns of response across development, we employed a
356 weighted-gene co-expression network approach, from data obtained at the
357 transcriptome level using all expressed genes (genes with low expression were not
358 considered, see Methods). This allowed us to build a network composed of 27 modules
359 with different sizes (ranging from 58 to 3970 genes) and with distinct expression
360 patterns (Figure 4, A and B; Supplemental Figure S5; Supplemental Data Set S7).

361 Within each individual module, we looked for genes with a significant time,
362 treatment, or time × treatment interaction effect (described in Figure 3A) or with a
363 specific or amplified response under WD/S- (identified in Figure 3H). We also explored
364 the repartition of transcriptional regulators within modules, after annotating them using
365 PlantTFcat (Supplemental Data Set S8). An enrichment analysis revealed 12 modules
366 that were significantly enriched for genes with a treatment effect (Figure 4C), which we

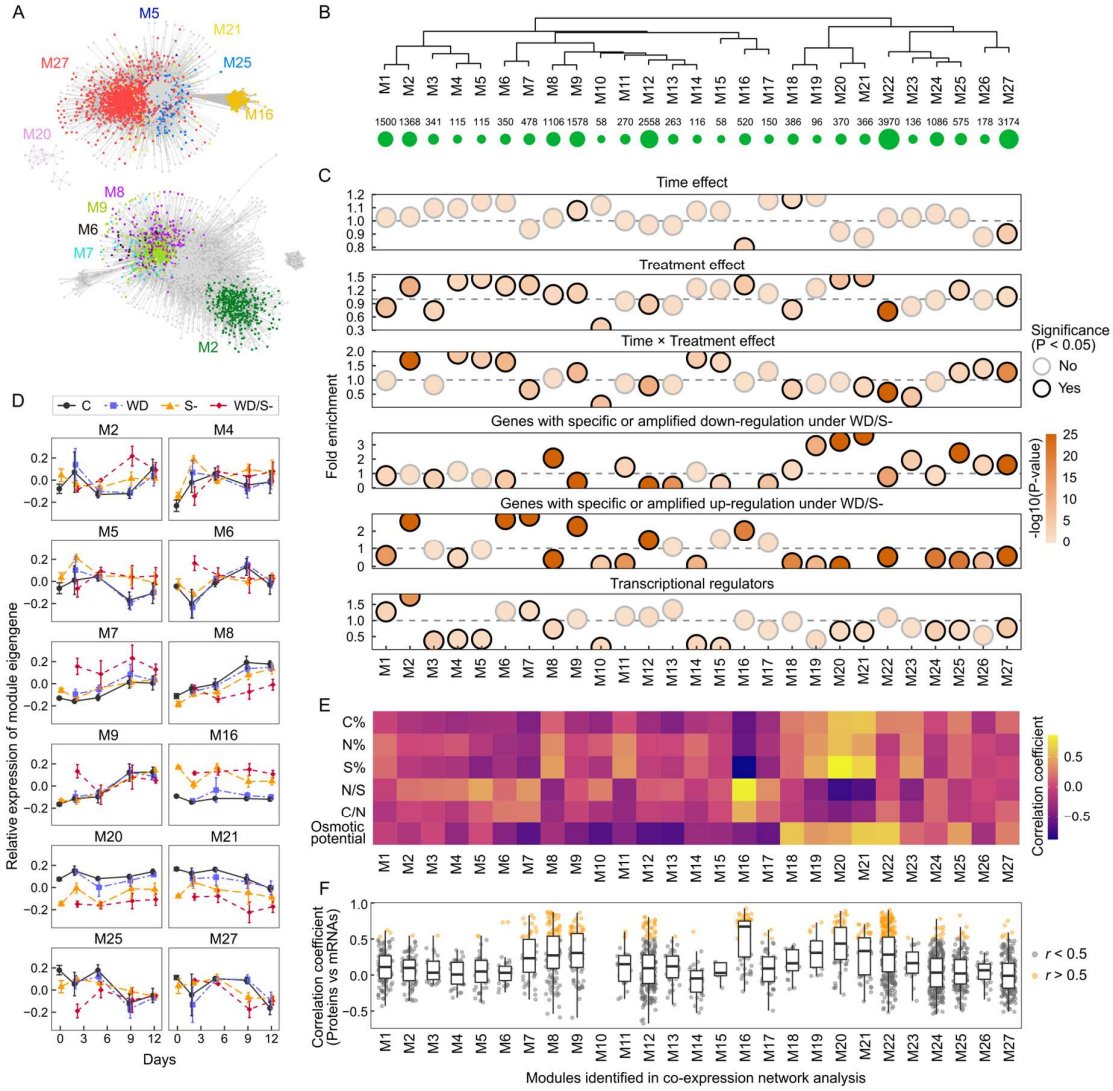

Figure 4. Identification of treatment-driven modules with specific patterns of response to stress using a co-expression network analysis. A, Co-expression network generated with WGCNA and visualized in Cytoscape using a Prefuse Force Directed layout, with an edge threshold cutoff of weight > 0.15. This network was built from transcriptomics data. Colored modules correspond to treatment-driven modules identified in C and presented in D. B, Clustering of module eigengenes. The module eigengene is defined as the first principal component of a given module (Langfelder and Horvath, 2008). The number of genes assigned to each module is indicated below the module name and represented as a bubble plot. C, Bubble plots representing enrichment of specific groups of genes within each module. Fold enrichment < 1 and > 1 correspond to an under- and over-representation in the module, respectively. Significance ($P < 0.05$, Fisher's exact test) is indicated as bubbles circled in black. Genes with a time, treatment and/or time × treatment interaction effects were identified in Figure 3A. Genes with a specific or amplified response in WD/S- at one or more time points are highlighted in Figure 3H. Transcriptional regulators were identified using the PlantTFCat tool. The absence of bubbles in certain modules is attributed to missing values (*e.g.* no genes with specific or amplified down-regulation under WD/S- were found in module M7, M10 and M16). D, Profiles of module eigengenes for modules significantly enriched for genes with a significant treatment effect (identified in C; means ± S.D, $n = 4$ replicates). Note that module M4 is not represented in A, because of the edge threshold cutoff used for the network visualization. E, Heatmap representing correlations (Spearman) between trait data (elements and osmotic potential) and module eigengenes. F, Boxplots showing the distribution by module of correlation (Spearman) coefficients for the comparison protein vs mRNA. Dots represent individual genes. Genes with a correlation > 0.5 (Protein vs mRNA) are highlighted in orange. Boundaries of the boxes represent the 25th and 75th percentiles, and horizontal lines within boxes represent medians.

390 selected and defined as treatment-driven modules (Figure 4D). Ten of these 12
391 modules were enriched for genes exhibiting a specific or amplified response under
392 WD/S-, and were either up-regulated (M2, M6, M7, M9, M16) or down-regulated (M8,
393 M20, M21, M25, M27) under this condition (Figure 4C). Hence, the selected treatment-
394 driven modules are representative of the greater response induced by the stress
395 combination, described above (Figure 3). In addition, some of these modules (M2, M4,
396 M5, M6, M9, M25, M27) were also enriched for genes with a significant time ×
397 treatment interaction effect, and therefore constitute interesting targets for analyzing
398 the influence of time on the stress response (Figure 4, C and D).
399 Correlations between modules and the accumulation of selected elements (C, N,
400 S, N/S and C/N) and osmotic potential were then calculated (Figure 4E). This revealed
401 that module M16 was highly correlated with these variables, particularly with S content
402 (negatively), and the N/S ratio (positively, Figure 4E). Genes within M16 were highly
403 expressed under both S- and WD/S-, as opposed to control and WD, across all time
404 points (Figure 4D). Module M20 showed the opposite pattern of expression and
405 therefore showed high correlation coefficients with the same variables (with opposite
406 signs of correlation coefficients, Figure 4, D and E). We hypothesized that modules
407 M16 and M20 are mainly driven by S availability and changes in the N/S ratio,
408 independently of water availability. Nonetheless, the over-representation of genes with
409 a specific or amplified response under WD/S- in both modules suggests that WD, when
410 combined with S deficiency, also contributes to the variation in gene expression within
411 these two modules (Figure 4D).
412 This co-expression network and the selected modules cover the main observations
413 made with statistical analyses, while shedding light on the diversity of gene expression
414 signatures in response to S deficiency with or without WD.
415

416 **A module of response to S deficiency reveals known and putative new regulators**
417 **of S-deficient conditions**

418 To better dissect the responses induced by S-, applied alone or with WD, we focused
419 on module M16, which grouped genes that were up-regulated in leaves in response to
420 both S- and WD/S- (Figure 4D). A Gene Ontology (GO) enrichment analysis evidenced
421 that several GO terms associated with sulfate assimilation and homeostasis,
422 biosynthesis of S compounds (Met, Cys, glutathione), and processes related to redox
423 homeostasis (*e.g.* 'response to reactive oxygen species', 'ascorbate glutathione cycle')

424 were significantly over-represented within M16 (Supplemental Figure S6;
425 Supplemental Data Set S5). We also found that two sulfate transporters (SULTRs)
426 were grouped into M16 and were up-regulated at most time points under both S- and
427 WD/S- (*Psat2g074400* and *Psat3g185920*; Supplemental Figure S7). *Psat2g074400*
428 is homologous to AtSULTR of group 1 involved in sulfate uptake and source to sink
429 transport in Arabidopsis (Yoshimoto et al. 2002) and *Psat3g185920* is homologous to
430 AtSULTR of group 4 involved in vacuolar sulfate efflux (Kataoka et al. 2004). This
431 suggests that S deficiency (occurring alone or combined with WD) may activate the
432 expression of genes involved in S transport and metabolism in leaves, possibly to
433 ensure the production of S-containing antioxidant molecules like glutathione and to
434 rebalance the availability of S and N.

435 Next, we selected genes with high module connectivity (module membership >
436 0.9) and strong negative correlation with S (gene significance for S < -0.9) within M16
437 (Figure 5A). In total, twenty-three genes were selected and designated as M16 hubs
438 (Figure 5, A and B; Supplemental Data Set S7). Two M16 hubs corresponded to
439 homologous genes of the OAS cluster gene *SULFUR DEFICIENCY INDUCED 1/2*
440 (*SDI1/2; Psat3g142720* and *Psat3g144280*). We then looked for other members and
441 found that all homologous genes of the Arabidopsis OAS cluster that were expressed
442 in our experiment (nine in total) were highly induced under both S- and WD/S- and
443 were grouped within module M16 (Supplemental Figure S8). Although only homologs
444 of *SDI1/2* were identified as hubs using our criteria, seven of the nine homologs
445 showed a module membership > 0.9 (Figure 5C). Interestingly, we also found that all
446 of the ten genes encoding proteins that were up-regulated under S- and WD/S- in
447 seeds in Henriet et al. (2021) were grouped in M16, with a high module membership
448 (> 0.9, Figure 5C). Six of them are M16 hubs and include a thioredoxin (*Psat5g207000)*
449 and a glutathione S-transferase (GST, *Psat6g125080*; Figure 5B). Together, these
450 results highlight a potential conservation of the molecular responses to S deficiency
451 between plant species (Arabidopsis and pea for the OAS cluster genes) and between
452 tissues (leaves and seeds in pea), and demonstrates the robustness of our network
453 analysis.

454 Module M16 was also the module with the highest overall correlation between
455 mRNA and protein data (Figure 4F). In fact, the distribution of correlation coefficients
456 (proteins vs mRNAs) within M16 was significantly different and higher (median = 0.672)
457 as compared to other modules (median = 0.119; Supplemental Figure S9). This

458 corroborates the enrichment of processes associated with the biosynthesis of S-
459 containing molecules within the group of 308 genes with a Protein/mRNA correlation
460 greater than 0.5 (Figure 3I). In addition, we performed a co-expression network
461 analysis from proteomic data, using the same methodology as for transcriptomic data.
462 A network of nine modules was built, in which module MP1 was identified as a
463 treatment-driven module, correlated with both S content and the N/S ratio, and
464 exhibiting an accumulation profile similar to M16 (Supplemental Figure S10). This
465 module was enriched for pathways also revealed in M16, including S-related
466 processes (*e.g.* sulfate assimilation) and processes associated with redox
467 homeostasis (Supplemental Figure S11). Hence, the list of genes within module M16
468 greatly overlaps with the list of genes encoding the proteins found in module MP1
469 (Supplemental Figure S12). Such overlap was not observed for other modules of co-
470 expression (Supplemental Figure S12). To illustrate, a homologous gene of the OAS
471 cluster gene *APR3* (*Psat1g179680*) and four M16 hub genes showed similar profiles
472 between mRNAs and proteins, with an up-regulation under S- and WD/S- as compared
473 to control and WD (Supplemental Figures S8 and S13). Altogether, these results
474 suggest that genes within M16 may be more strongly regulated at the transcriptional
475 level and less subjected to post-transcriptional regulations, as compared to genes
476 found in other modules.

477 To identify potential regulators of genes grouped in module M16 – and in other
478 modules of co-expression – we searched for predicted regulatory connections between
479 transcription factors (TFs, regulators) and their target genes using a gene regulatory
480 network inference approach. To limit the number of predicted connections, both
481 regulators and targets were restricted to proteins or mRNAs that were significantly
482 affected by treatments (identified in Figure 3A). In total, this approach identified 6508
483 regulatory connections between 102 TFs and 4830 target genes (Supplemental Figure
484 S14; Supplemental Data Set S7). For module M16, 55 TFs were predicted to target
485 160 genes in total (Figure 5, D and E). A group of seven regulators have a higher
486 number of targets and are central to a regulatory module, composed of 21 of the 23
487 identified M16 hubs and of five orthologs of the Arabidopsis OAS cluster genes (Figure
488 5, D and E). The TF with the highest number of targets within M16 (45) corresponds to
489 a member of the MYB/SANT family (*Psat0s2726g0040*), and is predicted to regulate
490 all five OAS cluster genes found in this module (Figure 5, D and E; Supplemental Data
491 Set S7).

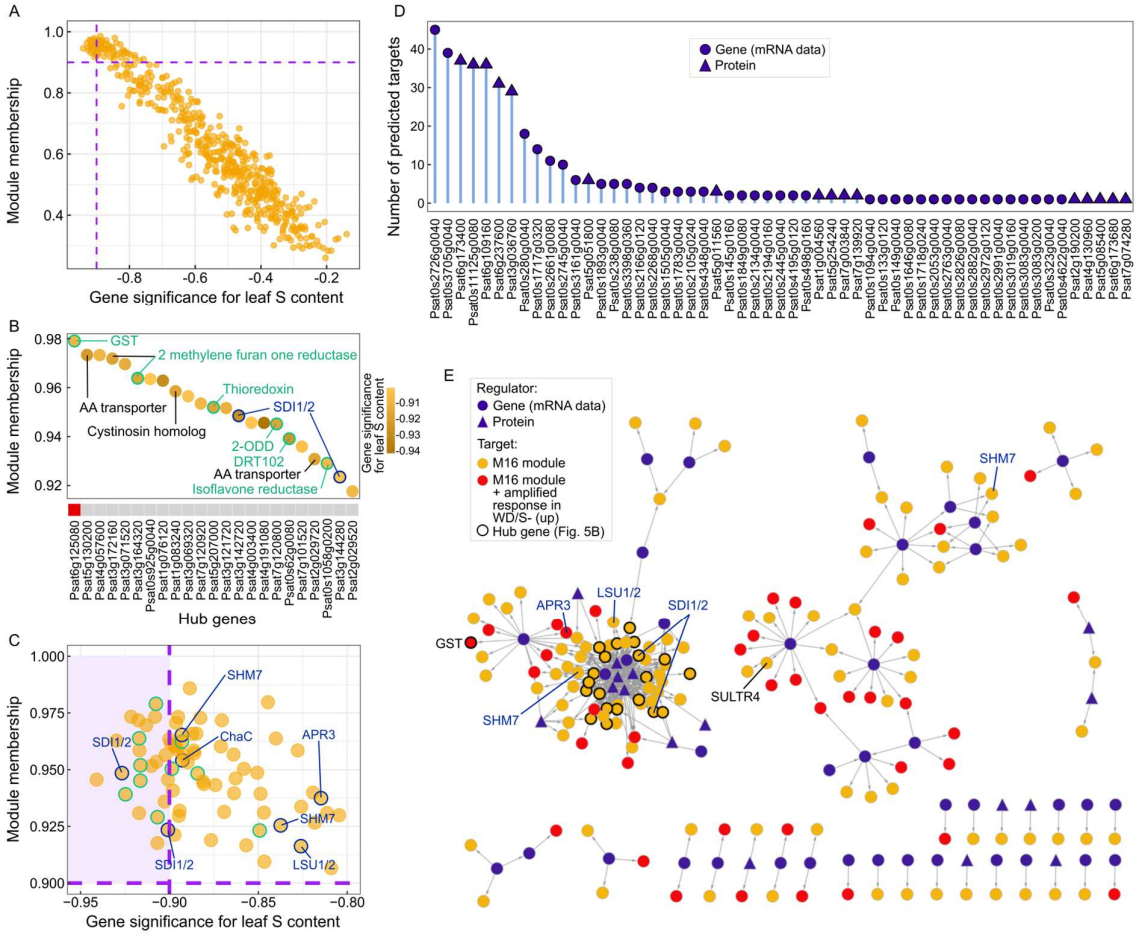

Figure 5. The M16 module reveals known and putative new regulators of response to sulfur deficiency (S-) combined or not with water deficit. A, Scatter plot of module membership vs gene significance for leaf S content in module M16. The horizontal and vertical purple dashed lines represent a module membership = 0.9 and a gene significance = -0.9, respectively. B, Dot plot ranking hub genes according to their module membership. Above gene IDs, red squares denote genes with amplified up-regulation under WD/S-, while grey squares represent genes without such amplified effect. C, Zoom of the scatter plot presented in A. The purple area delimits selected hub genes (gene significance < -0.9 and module membership > 0.9). In B and C, homologs of OAS cluster genes and genes encoding proteins that were up-regulated in pea seeds under S- and WD/S- in Henriet et al. (2021) are highlighted with black and green border lines, respectively. D, Predicted regulators of genes belonging to module M16. Regulators are TFs and correspond to proteins or mRNAs (when data for the TF was not available at the proteome level). Regulatory links were predicted using the method dynGENIE3. E, Regulatory network of M16 genes and their predicted regulators. Edges are oriented from regulators to target genes. M16 genes with an amplified up-regulation under WD/S- (identified in Figure 3F) are highlighted in red. AA, amino acid; GST, glutathione S-transferase; 2-ODD, bi-functional coumaroyl CoA and feruloyl CoA ortho-hydroxylase; DRT102, DNA damage repair toleration DRT.

Most of the M16 hubs were predicted to be targeted by multiple TFs and were found in the largest regulatory module (Figure 5E). Although most of them were strongly driven by S availability, independently of water availability, *Psat6g125080* – encoding a GST and identified as the M16 hub with the highest module membership (0.98, Figure 5B) – showed an amplified up-regulation under WD/S- (Figure 5C). Other

515 genes in M16 were specifically or more highly induced under WD/S- and include
516 homologs of the OAS cluster genes *APR3* (*Psat4g006280*) and *ChaC* (*Psat6g042040*;
517 Figure 5E; Supplemental Data Set S6). This suggests that stress combination
518 amplified the core mechanisms of response to S deficiency.
519
520 **Responses to stress combination are coordinated over time**
521 We reasoned that genes exhibiting a specific or amplified up-regulation under WD/S-
522 may correspond to genes important for the plant survival under this condition, which
523 severely compromised plant growth (Figure 1). We selected three contrasted
524 treatment-driven modules of co-expression, M2, M7 and M9, which were enriched for
525 genes with a specific or amplified up-regulation under WD/S-, and with different kinetics
526 of response (Figures 4D and 6A). Genes in M9 were specifically up-regulated at day 2
527 under WD/S-, as illustrated for hub genes within this module (Figure 6B). Genes in
528 module M2 exhibited an amplified up-regulation in response to WD/S- (as compared
529 to S-) at the end of the combined stress period (Figure 6, A and B). In addition, both
530 M2 and M9 were enriched for genes with a significant time × treatment interaction
531 effect (Figures 4C and 6B). These two modules can therefore be defined as time-
532 specific modules of response to WD/S-. In contrast, genes in module M7 did not
533 respond to WD/S- in a time-specific manner, and were up-regulated from day 2 to day
534 9 (Figure 6, A and B). Selected modules therefore showed unique gene expression
535 signatures under stress combination, with early (M9, day 2), late (M2, day 9), or early
536 to late (M7, day 2 to 9) responses (Figure 6A).
537 To identify biological pathways specifically activated early and/or lately under
538 WD/S-, we compared enriched GO terms within modules M2, M7 and M9
539 (Supplemental Figure S15, Supplemental Data Set S5). First, this analysis revealed
540 that genes up-regulated at multiple time points (module M7) play a role in responses
541 to various stresses (*e.g.* heat, salt, UV, hypoxia, Supplemental Data Set S5), including
542 the response to cadmium (Supplemental Figure S15). This suggests that module M7
543 corresponds to general stress-responsive genes, that may be activated under high
544 stress intensity and that remain highly expressed if the stress continues. Second, we
545 observed that M9 and M2 showed very specific GO enrichment results (Supplemental
546 Figure S15). More specifically, module M9 is characterized by genes involved in signal
547 transduction, protein phosphorylation, responses to oxidative stress and to hormones,
548 as well as in the response to abiotic stress and in defense-related processes (Figure

549 6C; Supplemental Figure S15). On the other hand, module M2 is highly represented
550 by genes with a role in the regulation of chromatin accessibility and gene expression
551 (Figure 6C; Supplemental Figure S15). In addition, some epigenetic-related GO terms
552 like 'chromatin remodeling' and 'regulation of gene expression, epigenetic' are
553 specifically enriched in module M2, considering all modules of co-expression (M1 to
554 M27; Supplementary Figure S16). Taken together, these results suggest that cascades
555 of signalization are induced in leaves from the first two days following the beginning of
556 stress combination to turn on stress-responsive genes, some of which remaining
557 activated up to the recovery period, whereas changes in chromatin accessibility
558 operate after several days under high stress intensity.

559 We next asked whether modules M2 and M9, which showed very distinct timing of
560 response, were regulated by specific TFs or TF families. Using results of the gene
561 regulatory network inference (Supplemental Figure S14), we observed that some TF
562 families were predicted to preferentially regulate module M2 or M9. For instance, three
563 bZIP members were identified as putative regulators of modules M2, M7 and M9, with
564 most of their targets located in M9 (Figure 6C). Similarly, the NAM and Hap3/NF-YB
565 families were predicted to mainly regulate genes from module M2 (Figure 6C). One of
566 the bZIPs (*Psat0s3019g0160*), which we renamed R1, was predicted to target 56
567 (29%) M9 hubs, and was identified as the highest ranked regulator in terms of number
568 of predicted targets (overall, using all modules of co-expression, Supplemental Figure
569 S14). This gene is homologous to the Arabidopsis gene *SULPHATE UTILIZATION*
570 *EFFICIENCY 3* (*SUE3/VIP1, AT1G43700*). In Arabidopsis, the *sue3* mutant displayed
571 enhanced tolerance to sulfur deficiency and to heavy metals and oxidative stress (Wu
572 et al. 2010). In our data, this gene was induced under WD/S- at days 5 and 9 (Figure
573 6D), and may thus act as a repressor of module M9, which showed an early response
574 (day 2) to this stress condition. R1 is also predicted to regulate genes from module M2
575 (Figure 6C; Supplemental Data Set S7), which are related to changes in chromatin
576 accessibility and which showed similar expression profiles as R1. Thus, R1 could be a
577 positive regulator of M2 genes. In that connection, using DAP-Seq data published for
578 Arabidopsis (O'Malley et al. 2016) and GO information, we found that genes involved
579 in epigenetic regulation of gene expression and in various developmental processes
580 were over-represented within the set of genes identified as AtSUE3 targets
581 (Supplemental Figure S17).
582

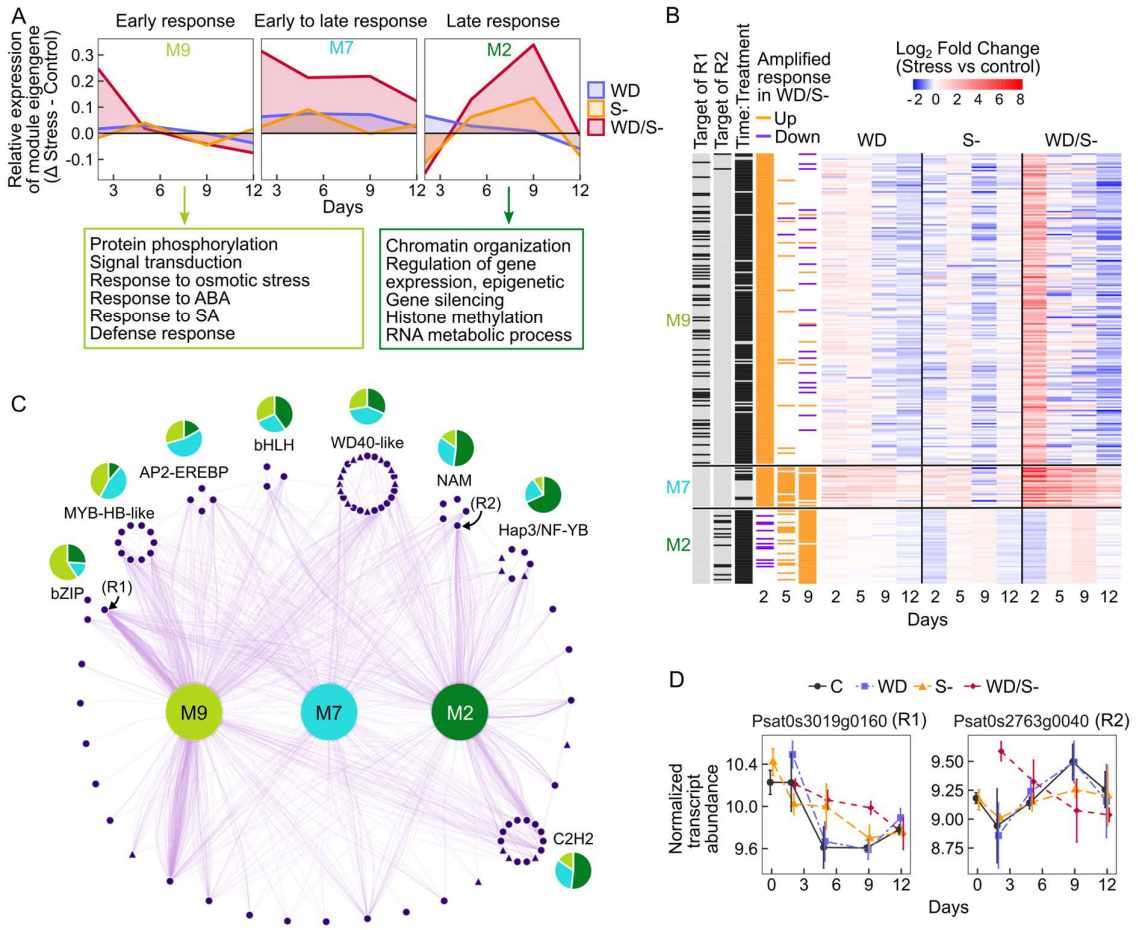

Figure 6. Modules of response to the stress combination show different timings of response. A, Area charts representing the average changes in relative expression of module eigengenes under stress conditions (Δ stress - control) for modules M9, M7 and M2. Below charts, selected enriched biological processes within modules M9 and M2 are indicated. B, Heatmap of hubs (module membership > 0.9) identified in modules M9, M7 and M2. The first three columns indicate whether (black) or not (grey) genes were identified as targets of R1 and R2 (highlighted in D and E) and/or showed a significant time × treatment interaction effect (Figure 3A). The next three columns highlight genes with a specific or amplified response under WD/S- as compared to single stress conditions (identified in Figure 3E). The last 12 columns represent changes in gene expression under stress as compared to control. Blue and red colors indicate lower and higher values in the stress condition as compared to control, respectively. C, Regulatory network of modules M9, M7 and M2 and their predicted regulators. Edges are oriented from regulators to target genes. Regulators are grouped by TF family. For TF families with at least three members, the proportion of modules M9, M7 and M2 within the predicted targets are represented as pie charts. Regulators R1 and R2 shown on Figure 6D are highlighted. D, Gene expression profiles of TFs R1 and R2 (means ± S.D, n = 4 biological replicates).

Most regulators were predicted to target genes from multiple modules. For example, a NAM member referred to as R2 (*Psat0s2763g0040)* is predicted to regulate hubs from both modules M2 and M9 (Figure 6, B and C). This gene is homologous to the Arabidopsis gene *SUPPRESSOR OF GAMMA RESPONSE 1* (*SOG1*, *AT1G25580*), a plant-specific transcriptional regulator that plays a major role in the

605 response to DNA damage (Preuss and Britt 2003; Yoshiyama et al. 2009). R2 was
606 specifically up-regulated at day 2 under WD/S-, then at day 9 its expression was lower
607 than under other three treatments. This regulator may therefore be a positive regulator
608 of module M9 (early response to the combined stress) and a repressor of module M2
609 (late response).

610 Our results suggest that responses to stress combination are tightly coordinated
611 over time, involving transcriptional regulators that may selectively activate and repress
612 specific pathways in a time-specific manner.

613

614 **Discussion**

615 Stress combination can lead to unique molecular responses in plants, which could not
616 be predicted from the effects observed under each individual stress. Here, we focused
617 on the responses of pea to S- and WD, and investigated how the combination of
618 stresses could accentuate the effects of single stresses or induce specific molecular
619 signatures.

620 Overall, combination of stresses caused important modifications of the plant
621 phenotype and leaf elemental composition, and of the leaf transcriptome and
622 proteome. When occurring alone, WD had a moderate effect on the measured
623 phenotypic variables, and fewer mRNAs and proteins were differentially accumulated
624 in leaves under this condition as compared to other treatments (Figure 1 and 3).
625 However, data collected at maturity on plants grown during the same experiment
626 showed that the number of reproductive nodes and the one-seed weight were
627 significantly reduced (Henriet et al. 2019). Hence, the plant responds to WD over the
628 long term while still recovering. During stress imposition and after three days of
629 rewatering, while WD had little effect when occurring alone, its strong impact when
630 combined with S- evidenced a synergistic effect between the two stresses. The leaf
631 osmotic potential at the end of the WD period (day 9, Figure 1) illustrates this
632 synergistic effect, with a 20% decrease under WD/S-, whereas it was decreased by
633 4.2% and 9.3% under WD and S-, respectively. In leaves, highest contents of iron, zinc
634 and cobalt were observed under the combined stress at days 9 and 12 (Figure 2,
635 Supplemental Figure S2). While these elements are essential for plants, their
636 hyperaccumulation can be detrimental to plant growth (Balafrej et al. 2020; Hu et al.
637 2021; Zahra et al. 2021). Similarly, leaf cadmium content was significantly higher at
638 the end of the experiment under WD/S- as compared to other treatments

639 (Supplemental Figure S2). Higher accumulation of these elements under the combined
640 stress could explain, at least in part, why the S-deficient plants did not survive an
641 additional three days of WD (Henriet et al. 2019).

642 Our co-expression network analysis evidenced a module of genes (M2) with an
643 amplified up-regulation under the combined stress at day 9, before plant rewatering,
644 when stress intensity was the highest. This module was enriched for genes involved in
645 chromatin organization and remodeling, as well as in epigenetic processes (Figure 6,
646 Supplemental Figure S16). The activation of genes playing a role in the regulation of
647 chromatin accessibility may reflect the activation of DNA damage responses (Casati
648 and Gomez 2021). Our network analyses revealed R2 (*Psat0s2763g0040*) as a
649 potential regulator of module M2, which is homolog to *SOG1* (*AT1G25580*), a plant-
650 specific transcriptional regulator that plays a major role in the response to DNA damage
651 (Preuss and Britt 2003; Yoshiyama et al. 2009). In pea leaves, *PsSOG1* was
652 specifically induced in the early response to the combined stress (Figure 6). Under this
653 condition that highly perturbed the plant development, we speculate that DNA
654 damages may occur, possibly due to ROS burst, which would activate the DNA repair
655 machinery through PsSOG1.

656 Single stresses have also caused alterations in the elemental composition of
657 leaves. This suggests that the uptake and transport of elements have been disrupted
658 by stress. Despite a drastic reduction in S contents in leaves under S-, either occurring
659 alone or in combination with WD, we identified two pea SULTR genes belonging to
660 module M16 that were highly up-regulated under S-limiting conditions (S- and WD/S-,
661 Supplemental Figure S7). These two transporters belong to groups 1 (*Psat2g074400*)
662 and 4 (*Psat3g185920*) implicated in sulfate uptake and efflux from the vacuole,
663 respectively, and may play an important role to limit the impact of S- in leaves. The two
664 S- conditions (S- and WD/S-) were also characterized by high molybdenum contents
665 in leaves (Figure 2). The increased uptake and accumulation of molybdenum when S
666 is limiting has been well documented in other crops (Shinmachi et al. 2010; Maillard et
667 al. 2016). Sulfate and molybdenum having similar biochemical properties,
668 molybdenum can be transported by sulfate transporters (Fitzpatrick et al. 2008). Of the
669 three molybdate transporters annotated in pea and expressed in our experiment, two
670 were grouped in the co-expression module M22 (*Psat5g026520* and *Psat6g031280*)
671 and did not respond to stress, and one (*Psat4g172720*) was grouped in the module
672 M20 and was down-regulated under S- and WD/S-. The increased content of

673 molybdenum in leaves under S- conditions could therefore result from an increased
674 transport by the two SULTR mentioned above. Similar results were observed in
675 *Brassica napus*, where S- induced higher molybdenum contents in leaves and strong
676 up-regulation of SULTR of group 1 in roots, whereas molybdate transporters showed
677 slight up-regulation or no differential expression (Maillard et al. 2016). Likewise, the
678 increased concentrations of toxic elements such as cadmium in pea leaves may result
679 from the activation of transporters of essential or beneficial nutrients (Zhao et al.
680 2022b). For instance, cadmium entry can be mediated by Mn transporters NRAMPs
681 (Cailliatte et al. 2010; Ishimaru et al. 2012; Sasaki et al. 2012) and by the Fe transporter
682 IRT1 (Vert et al. 2021).

683 While most DEGs were observed under S- and WD/S- conditions, suggesting a
684 high contribution of S availability to changes in gene expression, our analyses enabled
685 us to differentiate between genes primarily regulated by S availability and those
686 exhibiting specific or amplified responses to the combined stress. All expressed pea
687 homologs of the Arabidopsis OAS cluster were highly up-regulated under both S- and
688 WD/S-, with an up-regulation detected from day 0 (*i.e.* before WD imposition),
689 suggesting that their regulation by S deficiency is independent of water availability
690 (Figure 5, Supplemental Figure S8). However, orthologs of *APR3* (*Psat4g006280*) and
691 *ChaC* (*Psat6g042040*) showed an amplified up-regulation under stress combination as
692 compared to S deficiency applied alone (Figure 5; Supplemental Data Set S6). For
693 these genes, S availability may not be the only factor influencing their transcription.
694 Previous studies have shown that OAS cluster genes not only respond to S deprivation,
695 but also to other stresses where OAS accumulates, including conditions that generate
696 reactive oxygen species (ROS, Apodiakou and Hoefgen, 2023). Although ROS are by-
697 products of several metabolic processes, they accumulate under stress and can induce
698 oxidative stress, causing cellular damages. GO terms associated with responses to
699 ROS and redox homeostasis were enriched in both modules of response to S
700 deficiency (M16) and in modules of response to the combined stress (M7 and M9,
701 Supplemental Data Set S5). Analysis of module M16 revealed two hub genes encoding
702 enzymes with antioxidant roles, a GST (*Psat6g125080*) and a thioredoxin
703 (*Psat5g207000*), which showed similar patterns of response to stress at both mRNA
704 and protein levels (Figure 5, Supplemental Figures S12 and S13). Interestingly, these
705 two proteins were evidenced in pea seeds, in a cluster of antioxidant proteins that were
706 up-regulated in response to S- occurring alone or in combination with WD (Henriet et

707 al. 2021; Bonnot et al. 2023). This suggests that accumulation of ROS probably
708 occurred in both pea leaves and seeds of the treated pea plants, which activated
709 responses to oxidative stress involving similar key players between leaves and seeds.
710 Moreover, in leaves, the GST showed an amplified up-regulation under the combined
711 stress as compared to S deficiency applied alone (Figure 5), as also observed for
712 *PsAPR3* and *PsChaC* (mentioned above). We speculate that these three genes may
713 respond to stress intensity, which was higher under stress combination, whereas other
714 OAS cluster genes and other M16 hubs may rather respond to S availability.

715 Despite known connections between S assimilation and redox homeostasis
716 processes (reviewed in Bonnot et al., 2023), the extent to which these pathways share
717 similar regulatory mechanisms remains unclear. Using a gene regulatory network
718 approach, we identified a member of the MYB TF family, *Psat0s2726g0040*, which was
719 predicted to control the expression of most of the M16 hubs, several orthologs of the
720 Arabidopsis OAS cluster genes and genes with a role in the maintenance of the redox
721 balance (Figure 5; Supplemental Data Set S7). Recently, several TFs were proposed
722 to regulate an extended OAS cluster co-expression gene network in Arabidopsis, using
723 the Plant Regulomics database (Ran et al. 2020; Apodiakou and Hoefgen 2023).
724 These TFs included *AT3G10580*, a MYB related family member, that we found in the
725 same orthogroup as *Psat0s2726g0040* (Supplemental Table S1). This gene may
726 therefore represent an interesting candidate regulator of OAS cluster genes in plants
727 and, as suggested by our results in pea, of genes involved in redox homeostasis.

728 Among other interesting candidate regulators identified in our gene regulatory
729 network analysis, the gene R1, which is homolog to *SUE3/VIP1* (*AT1G43700)*, was
730 predicted to regulate a high number of genes (Figure 6). Our results suggested that it
731 may act as a repressor of genes activated in the early response to the combined stress
732 condition and involved in signaling and response to osmotic stress (module M9), and
733 as an activator of several genes with a late response and participating in the regulation
734 of chromatin accessibility (module M2). In Arabidopsis, SUE3/VIP1 was shown to bind
735 to the promoter of stress-responsive genes, activating their transcription, including
736 genes *TRXH8* (*AT1G69880*) and *MYB44* (Pitzschke et al. 2009). Thioredoxins-h type
737 (TRXH) are enzymes having an antioxidant function that are commonly induced in
738 plants in response to diverse stresses including drought and osmotic stress
739 (Schürmann and Jacquot 2000; Zhang et al. 2011; Chibani et al. 2021). Under drought
740 stress, MYB44 accumulates in Arabidopsis and participates in the increased

741 acetylation of H3K27 in stress-responsive genes, activating their transcription (Zhao et
742 al. 2022a). These previous findings support the hypothetical role of Ps-SUE3/VIP1 in
743 leaves, where it could play a pivotal role in the coordination of early vs late responses
744 to high stress intensity induced by multi-stress conditions.
745 We anticipate that our results pave the way for reverse genetic analyses of
746 selected candidate regulators, which may help modifying the plant capacity to induce
747 molecular responses to abiotic stresses under S-deprived conditions, in efforts to
748 improve crop tolerance to stress.
749

750 **Materials and methods**

751 **Plant growth, treatments and samplings**

752 Pea plants (*Pisum sativum* L., 'Caméor' genotype) were obtained from the experiment
753 described in (Henriet et al. 2019). Briefly, germinated seeds were sown in pots filled
754 with a mixture of perlite and sand (3/1, v/v). Plants were grown in a greenhouse, at
755 19°C/15°C (day/night) with a 16 h/8 h (light/dark) photoperiod. Plants were irrigated
756 with a nitrate- and S-rich (S+) solution containing 0.3 mM $MgSO_4 \cdot 7\ H_2O$ as a source
757 of S (Henriet et al., 2019). After three weeks (5/6 node stage), S- treatment was applied
758 to half of the plants: the substrate was rinsed twice using deionized water and twice
759 using a S- nutritive solution depleted of $MgSO_4 \cdot 7\ H_2O$ but containing 1.16 mM $MgCl_2$,
760 then plants were watered using this solution until the end of the experiment. After eight
761 days following the beginning of S- treatment, all plants (including S+ plants) at the 8-
762 node stage (on the primary branch, secondary branches were removed across the
763 experiment) were moved to an automated Plant Phenotyping Platform for Plant and
764 Micro-organism Interactions (4PMI, Dijon, France). Plants were weighted and watered
765 four times a day to maintain a water-holding capacity of the substrate of 100%. At
766 flowering of the second/third flowering nodes (*i.e.*, 16 days after the onset of S
767 deficiency), half of the plants (half of the S+ and half of the S deficiency-treated plants)
768 were subjected to WD: irrigation was stopped to reach a water-holding capacity of the
769 substrate of 50%, then this value was maintained for nine days. This level of irrigation
770 corresponded to a leaf water potential of -1.3 MPa (Henriet et al., 2019). After nine
771 days, plants were rewatered normally, with their respective nutritive solution (S+ or S-
772). This experimental setup allowed to get four different sets of plants, grown under:
773 control (no stress applied) condition, S-, WD, or a combination of S- and WD.
774

775 **Sampling and phenotypic and physiological measurements**

776 Sampling and measurements were performed on days 0, 2, 5, 9 and 12 after the start
777 of the WD application. Note that day 12 corresponds to three days after the end of WD,
778 *i.e.* three days of re-watering for the WD and WD/S conditions. A total of eigth plants
779 per condition and time point were grown and used for all experiments described below.

780 For leaf area measurements, the leaves of each individual plant were spread out
781 and scanned with an EPSON GT20000 (model J151A) scanner, and leaf area was
782 measured using a custom image processing algorithm. Dry weight measurements
783 were performed after drying tissues at 80°C for 48 h.

784 For osmotic potential estimation, leaflets from the last fully expanded leaves of
785 two independent plants were collected, placed in a syringe, frozen in liquid nitrogen
786 and stored at –80°C. After thawing, the cell sap was pressed out of a syringe, collected
787 and centrifuged at 10,000 × g for 10 min at 4°C. The osmolality of the corresponding
788 supernatant was measured using a vapour pressure osmometer (Wescor model 5520,
789 Bioblock Scientific, Illkirch, France), and the osmotic potential (MPa) was then
790 calculated according to the Van't Hoff equation: $\pi=(-R\times T\times \text{osmolality of the extract})$,
791 where T is the absolute temperature and R is the constant of perfect gas.

792 For -omics analyses, leaves were collected from the first two reproductive nodes
793 of two independent plants and pooled, resulting in four replicates. Samples were snap-
794 frozen in liquid nitrogen and stored at -80°C. The same samples were used for
795 transcriptomics, proteomics, ionomics and SCN content determination (see below).

796

797 **Element analyses**

798 S, C and N contents were determined from dried ground leaf samples (four biological
799 replicates) using the Dumas method (Allen et al. 1974). Contents of C and N were
800 determined from 5 mg of tissue powder on a Flash 2000 Elemental Analyzer (Thermo
801 Fisher Scientific), and contents of S were determined from 20 mg of tissue powder
802 mixed with 5 mg of tungsten trioxide on an elemental PYRO cube analyzer
803 (Elementar). Two technical replicates per biological replicate were performed.

804 Elements referred to as 'Ionomics data' in the manuscript correspond to essential
805 macro-nutrients (phosphorus, potassium, calcium, magnesium), micro-nutrients (iron,
806 boron, manganese, zinc, copper, molybdenum, nickel) and other elements (cobalt,
807 cadmium, lead, arsenic, vanadium), quantified by HR ICP-MS (Thermo Scientific,
808 Element 2TM). For each sample, 40 mg of dried ground leaf material were

809 resuspended in 800 µL of concentrated HNO_3, 200 µL H_2O_2 and 1 mL of Milli-Q water.
810 All samples were then spiked with three internal standard solutions containing gallium,
811 rhodium and iridium with final concentrations of 5, 1 and 1 µg L^{-1}, respectively. After
812 microwave acidic digestion (Multiwave ECO, Anton Paar, les Ulis, France), all samples
813 were diluted with 50 mL of Milli-Q water to obtain solutions containing 2.0% (v/v) nitric
814 acid. Before HR ICP-MS analysis, samples were filtered through a 0.45 µm teflon
815 filtration system (Digifilter, SCP Science, Courtaboeuf, France). Quantification of each
816 element was performed using external standard calibration curves and concentrations
817 were expressed in $\mu g.g^{-1}$ of leaves.
818
819 **Shotgun proteomics**
820 Protein sample preparation, analysis by LC-MS/MS and quantification, were performed
821 as described in (Henriet et al. 2021). Briefly, total proteins were extracted from 110 mg
822 of ground leaf tissues. Protein samples were lyophilized, then solubilized in buffer
823 containing 6 M urea, 2 M thiourea, 10 mM DTT, 30 mM Tris-HCl pH 8.8 and 0.1%
824 zwitterionic acid labile surfactant. For each sample, 20 µg of proteins were alkyled then
825 digested overnight at 37°C using trypsin. Trypsin-digested proteins were desalted and
826 analyzed by LC-MS/ MS using an Eksigent nlc425 device coupled to a Q Exactive
827 mass spectrometer (ThermoFisher Scientific), with a glass needle (non-coated
828 capillary silica tips, 360/20-10, New Objective). Proteins were identified using
829 X!Tandem v.2015.04.01.1 (Craig and Beavis 2004), by matching peptides against the
830 *P. sativum* v.1a database (https:// urgi.versailles.inra.fr/jbrowse/gmod_jbrowse/;
831 (Kreplak et al. 2019). Identified proteins were filtered and grouped using the
832 X!TandemPipeline software v.3.4.3 (Langella et al. 2017). Relative protein
833 quantification was performed using the MassChroQ software v.2.2 (Valot et al. 2011).
834 Protein quantification data is provided in Supplemental Data Set S3.
835
836 **RNA extraction and sequencing**
837 Extraction of RNAs from leaf tissues, RNA-sequencing (RNA-Seq) and data
838 processing were performed as described in (Henriet et al. 2019). Briefly, total RNAs
839 were extracted from ground leaf tissues using an RNeasy Plant Mini Kit (QIAGEN),
840 then a DNAse treatment with an RNase-Free DNase Set (QIAGEN) and a purification
841 step using lithium chloride precipitation were performed. RNA quality was checked on
842 a 2100 Bioanalyzer (Agilent Genomics). RNA-Seq libraries were prepared using an

843 Illumina TruSeq Stranded mRNA sample prep kit, and 11 PCR cycles were performed
844 to amplify the libraries. Library quality was checked using a Fragment Analyzer (Agilent
845 Genomics) and libraries were sequenced on the Illumina HiSeq3000 to obtain 2×150
846 bp paired-end reads. Quality of raw reads was assessed using the FastQC v0.11.2
847 software (https://www.bioinformatics.babraham.ac.uk/projects/fastqc/). Trimming of
848 low-quality and adapter sequences was performed on raw reads using Trimmomatic
849 v0.32 (Bolger et al. 2014). Trimmed reads with less than 25 bp and unpaired reads
850 were removed. Filtered reads were mapped to the *P. sativum* v1a reference genome
851 (https://urgi.versailles.inra.fr/Species/Pisum/Pea-Genome-project), using the
852 alignment program HISAT2 v2.0.5 (Kim et al. 2015). Read counting was performed
853 using FeatureCounts v1.5.0-p3 (Liao et al. 2014) on gene annotation v1b (Henriet et
854 al. 2019). Only genes with at least 10 reads total in the experiment were considered
855 as expressed and were used for downstream analyses (29575 genes in total). Gene
856 expression was normalized using the VST transformation proposed by the DESeq2
857 package (Love et al. 2014). Gene expression data is provided in Supplemental Dataset
858 S3.
859
860 **Statistical analyses**
861 *Identification of variables significantly affected by treatments*
862 All statistical analyses were performed with the software program R v. 4.1.2 (R Core
863 Team 2022). To assess the influence of S deficiency at the beginning of the experiment
864 on phenotypic variables, on leaf CNS contents, and on the leaf osmotic potential,
865 unpaired Student's t-tests were performed to compare treatments S- and control at day
866 0. Significant difference between treatments was judged at P-value < 0.05.
867 For data collected from days 2 to 9, the effects of time, treatments and the
868 interaction between these main effects were analyzed using the following model:
869 design = ~ Time + Treatment + Time:Treatment. For transcriptomics, differential
870 expression analysis was performed from raw counts of the 29575 filtered genes that
871 were considered as expressed (see above). Likelihood ratio tests (LRTs) were
872 performed with the DESeq2 package (Love et al. 2014), using the model described
873 above. The LRT is conceptually similar to an analysis of variance (ANOVA) calculation
874 in linear regression (Love et al. 2014). For other -omics data, two-way ANOVAs were
875 performed for each individual variable using the aov() function. For all data,
876 significance of factors was judged at P < 0.05 after FDR correction using the

877 Benjamini–Hochberg procedure (Benjamini and Hochberg 1995). Comparisons of
878 treatments were then performed at each time point. For transcriptomics, pairwise
879 comparisons were realized using the DESeq2 package (Love et al. 2014). For other -
880 omics data, Tukey's honestly significant difference (HSD) mean- separation tests were
881 performed, using the TukeyHSD() function. Variables were considered as differentially
882 responding to treatments at a given time point (*e.g.* in response to S- as compared to
883 control at day 2) if they showed *i*) a significant treatment effect (FDR < 0.05, LRTs or
884 ANOVAs) and *ii*) a significant difference between treatments (FDR < 0.05, pairwise
885 comparisons for transcriptomics; adjusted P-value < 0.05, Tukey's HSD tests for other
886 -omics data). To consider as significant both variables with high or low magnitude of
887 change in response to stress, no cutoff was applied on Fold Change values.
888 For data obtained at day 12, the same procedure was employed as for the
889 analysis at days 2-9, with the following modification in the model used for LRTs
890 (transcriptomics) and ANOVAs (other -omics data): design = ~ Treatment. Statistical
891 results are provided in Supplemental Dataset S2.
892
893 *Enrichment analyses*
894 Gene Ontology (GO) enrichment analyses were conducted using the TopGO R
895 package v. 2.46.0 (Alexa and Rahnenfuhrer 2022), with the Elim method and Fisher's
896 exact tests. GO terms with a *P*-value < 0.01 were considered as significantly enriched
897 in the selected subset of genes. Results are provided in Supplemental Data Set S5.
898 The GO term enrichment analysis performed from Arabidopsis genes was computed
899 using the interface of The Arabidopsis Information Resource for GO enrichment
900 analyses for plants (https://www.arabidopsis.org/tools/ go_term_enrichment.jsp),
901 powered by the Panther classification system (Mi et al. 2019). Significantly enriched
902 GO terms were considered at FDR < 0.05 (Fisher's exact tests).
903 To identify the enrichment of specific sets of genes (with a time, treatment or
904 time:treatment effects, with an amplified response under the combined stress
905 condition, or transcriptional regulators) within network modules, Fisher's exact tests
906 were performed. Proportions of these specific sets of genes within each module were
907 compared to their proportions in all genes found in the network. Significant differences
908 were judged at $P < 0.05$. Results are provided in Supplemental Data Set S9.
909
910 *Correlation between proteomics and transcriptomics data*

911 For each expressed gene for which a protein was successfully quantified in shotgun
912 proteomics (2240 genes in total), correlations were calculated between protein and
913 mRNA data, with the R cor() function and the Spearman method. Two separate
914 analyses were performed: one using data obtained from all treatment conditions
915 (Figure 3G), and one that was conducted by treatment (Figure 3H). Correlation
916 coefficients are provided in Supplemental Data Set S6.
917
918 **Network analyses**
919 *Co-expression network*
920 Weighted Gene Co-expression Network Analyses were conducted with the R package
921 'WGCNA' v. 1.72-5 (Langfelder and Horvath 2008). Two separate analyses were
922 performed, from data obtained at the 1) transcriptome and 2) proteome levels. Prior to
923 analysis, transcriptomic data were filtered to remove genes with low expression values
924 that could introduce noise into the network analysis. Genes with raw counts > 10 in at
925 least 50% of the samples were considered for the analysis, which represents 21281
926 genes. Normalized genes expression values (after VST transformation) were then
927 used. No filtering was applied on proteomic data, all 2261 quantified proteins were
928 used for the analysis. Data obtained at days 0 (control and S- conditions), 2, 5, 9 and
929 12 were used. Adjacency matrices were built using a soft threshold power of 12 and
930 16 for the analyses performed from transcriptomic and proteomic data, respectively.
931 To identify modules of co-expression, the minimum module size was set at 30. Similar
932 modules were merged, using a dissimilarity threshold of 0.25. Module eigengene
933 values were used to represent module expression patterns. Module information is
934 provided in Supplemental Data Set S7. To identify pea transcriptional regulators,
935 PlantTFcat was run on proteins of the v1b pea genome annotation, using default
936 parameters (Jin et al. 2017). Results are provided in Supplemental Data Set S8. For
937 selected pea genes, homologous genes in Arabidopsis were identified using reciprocal
938 BLASTP search (https://plants.ensembl.org/Multi/Tools/Blast). The phylogeny of
939 sulfate transporters (SULTRs) was built from protein sequences, using the interactive
940 phylogenetics module of the Dicots PLAZA v5 database
941 (https://bioinformatics.psb.ugent.be/plaza/versions/plaza_v5_dicots/). The software
942 MUSCLE v. 3.8.31 and FastTree v. 2.1.7 were used for the multiple sequence
943 alignment and the phylogenetic tree, respectively.
944

Gene regulatory network

Regulatory connections between transcription factors and target genes were predicted using the dynamical Gene Network Inference with Ensemble of trees (dynGENIE3) method (Huynh-Thu and Geurts 2018). Genes with low expression values were filtered out prior to analysis, as described above for the co-expression network analysis. In addition, this analysis was restricted to genes that showed a significant treatment effect (Figure 3A). Transcriptional regulators that were annotated as “transcription factors” (PlantTFcat analysis, Supplemental Data Set S6) were selected as input. For these input genes, data obtained at the protein level were preferred, when available, otherwise transcriptomic data were used. Transcriptomic data were used for the set of target genes. In total, 1172 input genes – which included 40 proteins – and 14180 potential target genes were used for this analysis. Regulatory links with a weight > 0.01 were selected to build regulatory networks. Results are provided in Supplemental Data Set S7. Arabidopsis homologs of selected candidate regulators were identified using the Dicots PLAZA v5 database (https://bioinformatics.psb.ugent.be/plaza/versions/plaza_v5_dicots/).

Data visualization

Heatmaps were generated with the R package ‘pheatmap’ v. 1.0.12 (Kolde 2019). Venn diagrams were drawn using the R package ‘eulerr’ v. 7.0.1 (Larsson 2022). Enriched GO terms were represented as described in (Bonnot et al. 2019). Networks were visualized with the software ‘CYTOSCAPE’ v. 3.9.0 (Smoot et al. 2011), using a Prefuse Force Directed Layout. For co-expression networks (generated with WGCNA), links with a weight > 0.15 (transcriptome analysis) or a weight > 0.10 (proteome analysis) were used for visualization. All other plots were prepared using the R package ‘ggplot2’ v. 3.4.4 (Wickham 2016).

Data availability

Raw mass spectrometry files have been deposited to the ProteomeXchange Consortium via the PRIDE partner repository with the dataset identifier PXD048279. Raw RNA-Seq data (fasta files and read counting data) are accessible from the Gene Expression Omnibus (GEO) database, www.ncbi.nlm.nih.gov/geo, with the identifier GSE252351. All other data are available as Supplemental Data Sets.

979 **Supplemental data**

980 **Supplemental Table S1.** Arabidopsis genes identified in the same orthogroup
981 (ORTHO05D000330) as *Psat0s2726g0040*, according to the Dicots PLAZA v.5
982 database.

983 **Supplemental Figure S1**. Quantification of sulfur (S) in leaves: correlation between
984 the two quantification methods.

985 **Supplemental Figure S2**. Accumulation profiles of elements over time in leaves.

986 **Supplemental Figure S3**. Volcano plots representing statistical significance versus
987 magnitude of change for mRNAs.

988 **Supplemental Figure S4**. Selected enriched biological processes in the list of genes
989 with a specific or amplified down-regulation under WD/S- as compared to single stress
990 conditions.

991 **Supplemental Figure S5**. Profiles of module eigengenes for modules identified in the
992 co-expression network analysis, performed from transcriptomic data.

993 **Supplemental Figure S6**. Enriched biological processes in the list of 520 genes
994 grouped in module M16.

995 **Supplemental Figure S7**. Response to stress of sulfate transporters.

996 **Supplemental Figure S8**. Response to stress of OAS cluster genes.

997 **Supplemental Figure S9**. Distribution of correlation (Protein vs mRNA) coefficients
998 within M16 and other modules.

999 **Supplemental Figure S10**. Co-accumulation network of proteins reveals modules with
1000 distinct patterns of response to stress.

1001 **Supplemental Figure S11**. Enriched biological processes in the list of 333 proteins
1002 grouped in module MP1.

1003 **Supplemental Figure S12**. Overlap between co-expression modules (transcriptomics
1004 data) and co-accumulation modules (proteomics data).

1005 **Supplemental Figure S13**. Expression profiles (mRNAs and proteins) of selected
1006 hubs in module M16.

1007 **Supplemental Figure S14**. Prediction of regulatory connections between TFs and
1008 their target genes.

1009 **Supplemental Figure S15**. Selected enriched biological processes in modules M2,
1010 M7 and M9.

Supplemental Figure S16. Enrichment of biological processes related to epigenetic mechanisms in co-expression modules.

Supplemental Figure S17. Enriched biological processes within the list of genes targeted by AT1G43700, identified as homologous to the regulator R1.

Supplemental Data Set S1. Quantification results (Phenomics, osmotic potential, elements).

Supplemental Data Set S2. Statistical results.

Supplemental Data Set S3. Transcriptomics and proteomics data.

Supplemental Data Set S4. Correlations between proteins and mRNAs.

Supplemental Data Set S5. Gene Ontology enrichment analysis.

Supplemental Data Set S6. Genes with an amplified response under WD/S- as compared to single stress conditions.

Supplemental Data Set S7. Network results.

Supplemental Data Set S8. Transcription factors in *Pisum sativum.*

Supplemental Data Set S9. Enrichment of gene sets within modules.

Acknowledgments

We thank the members of the 4PMI Platform (Phenotyping Platform for Plant and Plant Microorganisms Interactions, INRAE, Dijon) for their excellent technical support during plant growth and all members of the FILEAS team for helping with sample collection and measurements of plants phenotypic variables. We also thank Mickaël Lamboeuf for the development of the custom image processing algorithm used for the calculation of the leaf surface area, Sylvie Girodet for CN measurements and the GISMO platform (Université de Bourgogne Franche-Comté, Dijon, France) for S measurements; Rémy-Félix Serre from the GeT-PlaGe core facility (Castanet-Tolosan, France) for the sequencing of mRNAs and pre-processing of the mRNA-Seq data. We also thank Marion Prudent for her help with the experimental setup, and Christine Le Signor for helpful discussions to interpret the data.

Funding

The PhD grant of CH was funded by the French Ministry for Higher Education and Research. Analyses were supported by the European Union (FP7 Program 'LEGATO', project n°613551, greenhouse experiments); by the INRAE Plant Breeding department

(project PRORESO, proteomics) and by the TIMAC Agro International - Groupe Roullier within the framework of the FUI-SERAPIS project (RNA-Seq).
Conflict of interest statement: The authors declare no competing interests.
For the purpose of open access, the authors have applied a CC-BY public copyright licence to any Author Accepted Manuscript (AAM) version arising from this submission.

References

Aarabi F, Kusajima M, Tohge T, Konishi T, Gigolashvili T, Takamune M, Sasazaki Y, Watanabe M, Nakashita H, Fernie AR, et al. Sulfur deficiency-induced repressor proteins optimize glucosinolate biosynthesis in plants. Science Advances. 2016:**2**(10):e1601087–e1601087. https://doi.org/10.1126/sciadv.1601087

Aarabi F, Rakpenthai A, Barahimipour R, Gorka M, Alseekh S, Zhang Y, Salem MA, Brückner F, Omranian N, Watanabe M, et al. Sulfur deficiency-induced genes affect seed protein accumulation and composition under sulfate deprivation. Plant Physiology. 2021:**187**(4):2419–2434. https://doi.org/10.1093/plphys/kiab386

Alexa A and Rahnenfuhrer J. topGO: Enrichment analysis for Gene Ontology. 2022.

Allen WM, Berrett S, and Patterson DSP. A biochemical study of experimental Johne's disease. Journal of Comparative Pathology. 1974:**84**(3):385–389. https://doi.org/10.1016/0021-9975(74)90013-9

Apodiakou A and Hoefgen R. New insights into the regulation of plant metabolism by O -acetylserine: sulfate and beyond. Journal of Experimental Botany. 2023:**74**(11):3361–3378. https://doi.org/10.1093/jxb/erad124

Azodi CB, Lloyd JP, and Shiu S-H. The cis-regulatory codes of response to combined heat and drought stress in Arabidopsis thaliana. NAR Genomics and Bioinformatics. 2020:**2**(3):1–16. https://doi.org/10.1093/nargab/lqaa049

Balafrej H, Bogusz D, Triqui Z-EA, Guedira A, Bendaou N, Smouni A, and Fahr M. Zinc Hyperaccumulation in Plants: A Review. Plants. 2020:**9**(5):562. https://doi.org/10.3390/plants9050562

Benjamini Y and Hochberg Y. Controlling the false discovery rate: a practical and powerful approach to multiple testing. Journal of the Royal Statistical Society Series B (Methodological). 1995:**57**:289–300. https://doi.org/10.2307/2346101

1077 **Bolger AM, Lohse M, and Usadel B**. Trimmomatic: a flexible trimmer for Illumina
1078 sequence data. Bioinformatics. 2014:**30**(15):2114–2120.
1079 https://doi.org/10.1093/bioinformatics/btu170
1080 **Bonnot T, Bachelet F, Boudet J, Le Signor C, Bancel E, Vernoud V, Ravel C, and**
1081 **Gallardo K**. Sulfur in determining seed protein composition: present
1082 understanding of its interaction with abiotic stresses and future directions.
1083 Journal of Experimental Botany. 2023:**74**(11):3276–3285.
1084 https://doi.org/10.1093/jxb/erad098
1085 **Bonnot T, Gillard M, and Nagel D**. A Simple Protocol for Informative Visualization of
1086 Enriched Gene Ontology Terms. Bio-101. 2019:e3429.
1087 https://doi.org/10.21769/BioProtoc.3429
1088 **Bonnot T, Martre P, Hatte V, Dardevet M, Leroy P, Bénard C, Falagán N, Martin-**
1089 **Magniette M-L, Deborde C, Moing A, et al.** Omics Data Reveal Putative
1090 Regulators of Einkorn Grain Protein Composition under Sulfur Deficiency. Plant
1091 Physiology. 2020:**183**(2):501–516. https://doi.org/10.1104/pp.19.00842
1092 **Borja Reis AF de, Rosso LHM, Davidson D, Kovács P, Purcell LC, Below FE,**
1093 **Casteel SN, Knott C, Kandel H, Naeve SL, et al.** Sulfur fertilization in soybean:
1094 A meta-analysis on yield and seed composition. European Journal of
1095 Agronomy. 2021:**127**:126285. https://doi.org/10.1016/j.eja.2021.126285
1096 **Cailliatte R, Schikora A, Briat J-F, Mari S, and Curie C**. High-Affinity Manganese
1097 Uptake by the Metal Transporter NRAMP1 Is Essential for Arabidopsis Growth
1098 in Low Manganese Conditions. The Plant Cell. 2010:**22**(3):904–917.
1099 https://doi.org/10.1105/tpc.109.073023
1100 **Casati P and Gomez MS**. Chromatin dynamics during DNA damage and repair in
1101 plants: new roles for old players. Journal of Experimental Botany.
1102 2021:**72**(11):4119–4131. https://doi.org/10.1093/jxb/eraa551
1103 **Chibani K, Pucker B, Dietz K, and Cavanagh A**. Genome-wide analysis and
1104 transcriptional regulation of the typical and atypical thioredoxins in Arabidopsis
1105 thaliana. FEBS Letters. 2021:**595**(21):2715–2730.
1106 https://doi.org/10.1002/1873-3468.14197
1107 **Cohen I, Zandalinas SI, Huck C, Fritschi FB, and Mittler R**. Meta-analysis of drought
1108 and heat stress combination impact on crop yield and yield components.
1109 Physiologia Plantarum. 2021:**171**(1):66–76. https://doi.org/10.1111/ppl.13203

Connolly EL and Guerinot ML. Iron stress in plants. Genome Biology. 2002:**3**(8):1–4. https://doi.org/10.1186/gb-2002-3-8-reviews1024

Craig R and Beavis RC. TANDEM: matching proteins with tandem mass spectra. Bioinformatics. 2004:**20**(9):1466–1467. https://doi.org/10.1093/bioinformatics/bth092

Detzel A, Krüger M, Busch M, Blanco-Gutiérrez I, Varela C, Manners R, Bez J, and Zannini E. Life cycle assessment of animal-based foods and plant-based protein-rich alternatives: an environmental perspective. Journal of the Science of Food and Agriculture. 2022:**102**(12):5098–5110. https://doi.org/10.1002/jsfa.11417

Fitzpatrick KL, Tyerman SD, and Kaiser BN. Molybdate transport through the plant sulfate transporter SHST1. FEBS Letters. 2008:**582**(10):1508–1513. https://doi.org/10.1016/j.febslet.2008.03.045

Haneklaus S, Bloem E, and Schnug E. History of Sulfur Deficiency in Crops. . In. Sulfur: A Missing Link between Soils, Crops, and Nutrition. (John Wiley & Sons, Ltd), pp. 45-58–6. https://doi.org/10.2134/agronmonogr50.c4

Henriet C, Aimé D, Térézol M, Kilandamoko A, Rossin N, Combes-Soia L, Labas V, Serre R-F, Prudent M, Kreplak J, et al. Water stress combined with sulfur deficiency in pea affects yield components but mitigates the effect of deficiency on seed globulin composition. Journal of Experimental Botany. 2019:**70**(16):4287–4304. https://doi.org/10.1093/jxb/erz114

Henriet C, Balliau T, Aimé D, Le Signor C, Kreplak J, Zivy M, Gallardo K, and Vernoud V. Proteomics of developing pea seeds reveals a complex antioxidant network underlying the response to sulfur deficiency and water stress. Journal of Experimental Botany. 2021:**72**(7):2611–2626. https://doi.org/10.1093/jxb/eraa571

Hu X, Wei X, Ling J, and Chen J. Cobalt: An Essential Micronutrient for Plant Growth? Frontiers in Plant Science. 2021:**12**(November):1–24. https://doi.org/10.3389/fpls.2021.768523

Hubberten H-M, Klie S, Caldana C, Degenkolbe T, Willmitzer L, and Hoefgen R. Additional role of O-acetylserine as a sulfur status-independent regulator during plant growth. The Plant Journal. 2012:**70**(4):666–677. https://doi.org/10.1111/j.1365-313X.2012.04905.x

1143 **Huynh-Thu VA and Geurts P**. dynGENIE3: dynamical GENIE3 for the inference of
1144 gene networks from time series expression data. Scientific Reports.
1145 2018:**8**(1):3384. https://doi.org/10.1038/s41598-018-21715-0
1146 **IPCC**. IPCC, 2023: Climate Change 2023: Synthesis Report. A Report of the
1147 Intergovernmental Panel on Climate Change. Contribution of Working Groups
1148 I, II and III to the Sixth Assessment Report of the Intergovernmental Panel on
1149 Climate Change (Geneva, Switzerland).
1150 **Ishimaru Y, Takahashi R, Bashir K, Shimo H, Senoura T, Sugimoto K, Ono K,**
1151 **Yano M, Ishikawa S, Arao T, et al.** Characterizing the role of rice NRAMP5 in
1152 Manganese, Iron and Cadmium Transport. Scientific Reports. 2012:**2**(1):286.
1153 https://doi.org/10.1038/srep00286
1154 **Jacques C, Forest M, Durey V, Salon C, Ourry A, and Prudent M**. Transient Nutrient
1155 Deficiencies in Pea: Consequences on Nutrient Uptake, Remobilization, and
1156 Seed Quality. Frontiers in Plant Science. 2021:**12**(December):1–14.
1157 https://doi.org/10.3389/fpls.2021.785221
1158 **Jin J, Tian F, Yang D-C, Meng Y-Q, Kong L, Luo J, and Gao G**. PlantTFDB 4.0:
1159 toward a central hub for transcription factors and regulatory interactions in
1160 plants. Nucleic Acids Research. 2017:**45**(D1):D1040–D1045.
1161 https://doi.org/10.1093/nar/gkw982
1162 **Kataoka T, Watanabe-Takahashi A, Hayashi N, Ohnishi M, Mimura T, Buchner P,**
1163 **Hawkesford MJ, Yamaya T, and Takahashi H**. Vacuolar Sulfate Transporters
1164 Are Essential Determinants Controlling Internal Distribution of Sulfate in
1165 Arabidopsis. Plant Cell. 2004:**16**(10):2693–2704.
1166 https://doi.org/10.1105/tpc.104.023960
1167 **Kim D, Langmead B, and Salzberg SL**. HISAT: a fast spliced aligner with low memory
1168 requirements. Nature Methods. 2015:**12**(4):357–360.
1169 https://doi.org/10.1038/nmeth.3317
1170 **Kolde R**. pheatmap: Pretty Heatmaps. 2019.
1171 **Kreplak J, Madoui M-A, Cápal P, Novák P, Labadie K, Aubert G, Bayer PE, Gali**
1172 **KK, Syme RA, Main D, et al.** A reference genome for pea provides insight into
1173 legume genome evolution. Nature Genetics. 2019:**51**(9):1411–1422.
1174 https://doi.org/10.1038/s41588-019-0480-1
1175 **Langella O, Valot B, Balliau T, Blein-Nicolas M, Bonhomme L, and Zivy M**.
1176 X!TandemPipeline: A Tool to Manage Sequence Redundancy for Protein

Inference and Phosphosite Identification. Journal of Proteome Research. 2017:**16**(2):494–503. https://doi.org/10.1021/acs.jproteome.6b00632

Langfelder P and Horvath S. WGCNA: an R package for weighted correlation network analysis. BMC Bioinformatics. 2008:**9**(1):559. https://doi.org/10.1186/1471-2105-9-559

Larsson J. eulerr: Area-Proportional Euler and Venn Diagrams with Ellipses. 2022.

Lecomte C, Richer V, Gauffreteau A, Jeuffroy MH, Bouviala M, Brun C, Buridan C, Klein A, Lantoine FX, Marchand D, et al. Combining a multi-environment trial and a diagnosis method to assess potential yield and main limiting factors of three highly different pea types. European Journal of Agronomy. 2023:**146**(April). https://doi.org/10.1016/j.eja.2023.126823

Liao Y, Smyth GK, and Shi W. featureCounts: an efficient general purpose program for assigning sequence reads to genomic features. Bioinformatics. 2014:**30**(7):923–930. https://doi.org/10.1093/bioinformatics/btt656

Love MI, Huber W, and Anders S. Moderated estimation of fold change and dispersion for RNA-seq data with DESeq2. Genome Biology. 2014:**15**(12):550. https://doi.org/10.1186/s13059-014-0550-8

Mahalingam R, Duhan N, Kaundal R, Smertenko A, Nazarov T, and Bregitzer P. Heat and drought induced transcriptomic changes in barley varieties with contrasting stress response phenotypes. Frontiers in Plant Science. 2022:**13**(December):1–24. https://doi.org/10.3389/fpls.2022.1066421

Maillard A, Etienne P, Diquélou S, Trouverie J, Billard V, Yvin J-C, and Ourry A. Nutrient deficiencies modify the ionomic composition of plant tissues: a focus on cross-talk between molybdenum and other nutrients in Brassica napus. Journal of Experimental Botany. 2016:**67**(19):5631–5641. https://doi.org/10.1093/jxb/erw322

Mi H, Muruganujan A, Ebert D, Huang X, and Thomas PD. PANTHER version 14: more genomes, a new PANTHER GO-slim and improvements in enrichment analysis tools. Nucleic Acids Research. 2019:**47**(D1):D419–D426. https://doi.org/10.1093/nar/gky1038

Mittler R. Abiotic stress, the field environment and stress combination. Trends in Plant Science. 2006:**11**(1):15–19. https://doi.org/10.1016/j.tplants.2005.11.002

1209 **Mondal S, Pramanik K, Panda D, Dutta D, Karmakar S, and Bose B**. Sulfur in
1210 Seeds: An Overview. Plants. 2022:**11**(3):450.
1211 https://doi.org/10.3390/plants11030450
1212 **O'Malley RC, Huang SC, Song L, Lewsey MG, Bartlett A, Nery JR, Galli M,**
1213 **Gallavotti A, and Ecker JR**. Cistrome and epicistrome features shape the
1214 regulatory DNA landscape. Cell. 2016:**165**(5):1280–1292.
1215 https://doi.org/10.1016/j.cell.2016.04.038
1216 **Paine RT, Tegner MJ, and Johnson E a**. Ecological Surprises. Ecosystems.
1217 1998:**1**(July):535–545.
1218 **Pitzschke A, Djamei A, Teige M, and Hirt H**. VIP1 response elements mediate
1219 mitogen-activated protein kinase 3-induced stress gene expression.
1220 Proceedings of the National Academy of Sciences. 2009:**106**(43):18414–
1221 18419. https://doi.org/10.1073/pnas.0905599106
1222 **Poisson E, Trouverie J, Brunel-Muguet S, Akmouche Y, Pontet C, Pinochet X,**
1223 **and Avice J-C**. Seed Yield Components and Seed Quality of Oilseed Rape Are
1224 Impacted by Sulfur Fertilization and Its Interactions With Nitrogen Fertilization.
1225 Frontiers in Plant Science. 2019:**10**. https://doi.org/10.3389/fpls.2019.00458
1226 **Poore J and Nemecek T**. Reducing food's environmental impacts through producers
1227 and consumers. Science. 2018:**360**(6392):987–992.
1228 https://doi.org/10.1126/science.aaq0216
1229 **Preuss SB and Britt AB**. A DNA-Damage-Induced Cell Cycle Checkpoint in
1230 Arabidopsis. Genetics. 2003:**164**(1):323–334.
1231 https://doi.org/10.1093/genetics/164.1.323
1232 **R Core Team**. R: A Language and environment for statistical computing. 2022.
1233 **Ran X, Zhao F, Wang Y, Liu J, Zhuang Y, Ye L, Qi M, Cheng J, and Zhang Y**. Plant
1234 Regulomics: a data-driven interface for retrieving upstream regulators from
1235 plant multi-omics data. The Plant Journal. 2020:**101**(1):237–248.
1236 https://doi.org/10.1111/tpj.14526
1237 **Rasmussen S, Barah P, Suarez-Rodriguez MC, Bressendorff S, Friis P,**
1238 **Costantino P, Bones AM, Nielsen HB, and Mundy J**. Transcriptome
1239 responses to combinations of stresses in *Arabidopsis*. Plant Physiology.
1240 2013:**161**(4):1783–1794. https://doi.org/10.1104/pp.112.210773
1241 **Ristova D and Kopriva S**. Sulfur signaling and starvation response in Arabidopsis.
1242 iScience. 2022:**25**(5):104242. https://doi.org/10.1016/j.isci.2022.104242

1243 **Rizhsky L, Liang H, and Mittler R**. The Combined Effect of Drought Stress and Heat
1244 Shock on Gene Expression in Tobacco. Plant Physiology. 2002:**130**(3):1143–
1245 1151. https://doi.org/10.1104/pp.006858
1246 **Rizhsky L, Liang H, Shuman J, Shulaev V, Davletova S, and Mittler R**. When
1247 defense pathways collide. The response of arabidopsis to a combination of
1248 drought and heat stress 1[w]. Plant Physiology. 2004:**134**(4):1683–1696.
1249 https://doi.org/10.1104/pp.103.033431
1250 **Samanta S, Singh A, and Roychoudhury A**. Involvement of Sulfur in the Regulation
1251 of Abiotic Stress Tolerance in Plants. . In. Protective Chemical Agents in the
1252 Amelioration of Plant Abiotic Stress. (Wiley), pp. 437–466.
1253 https://doi.org/10.1002/9781119552154.ch22
1254 **Sasaki A, Yamaji N, Yokosho K, and Ma JF**. Nramp5 Is a Major Transporter
1255 Responsible for Manganese and Cadmium Uptake in Rice. The Plant Cell.
1256 2012:**24**(5):2155–2167. https://doi.org/10.1105/tpc.112.096925
1257 **Scherer HW**. Sulphur in crop production. European Journal of Agronomy.
1258 2001:**14**(2):81–111. https://doi.org/10.1016/S1161-0301(00)00082-4
1259 **Schürmann P and Jacquot J-P**. PLANT THIOREDOXIN SYSTEMS REVISITED.
1260 Annual Review of Plant Physiology and Plant Molecular Biology.
1261 2000:**51**(1):371–400. https://doi.org/10.1146/annurev.arplant.51.1.371
1262 **Shinmachi F, Buchner P, Stroud JL, Parmar S, Zhao F-J, McGrath SP, and**
1263 **Hawkesford MJ**. Influence of Sulfur Deficiency on the Expression of Specific
1264 Sulfate Transporters and the Distribution of Sulfur, Selenium, and Molybdenum
1265 in Wheat. Plant Physiology. 2010:**153**(1):327–336.
1266 https://doi.org/10.1104/pp.110.153759
1267 **Smoot ME, Ono K, Ruscheinski J, Wang P-L, and Ideker T**. Cytoscape 2.8: new
1268 features for data integration and network visualization. Bioinformatics.
1269 2011:**27**(3):431–432. https://doi.org/10.1093/bioinformatics/btq675
1270 **Stagnari F, Maggio A, Galieni A, and Pisante M**. Multiple benefits of legumes for
1271 agriculture sustainability: an overview. Chemical and Biological Technologies in
1272 Agriculture. 2017:**4**(1):2. https://doi.org/10.1186/s40538-016-0085-1
1273 **Tan JW, Shinde H, Tesfamicael K, Hu Y, Fruzangohar M, Tricker P, Baumann U,**
1274 **Edwards EJ, and Rodríguez López CM**. Global transcriptome and gene co-
1275 expression network analyses reveal regulatory and non-additive effects of

1276 drought and heat stress in grapevine. Frontiers in Plant Science.
1277 2023:**14**(February):1–15. https://doi.org/10.3389/fpls.2023.1096225
1278 **Valot B, Langella O, Nano E, and Zivy M**. MassChroQ: A versatile tool for mass
1279 spectrometry quantification. PROTEOMICS. 2011:**11**(17):3572–3577.
1280 https://doi.org/10.1002/pmic.201100120
1281 **Varshney RK, Pandey MK, Bohra A, Singh VK, Thudi M, and Saxena RK**. Toward
1282 the sequence-based breeding in legumes in the post-genome sequencing era.
1283 Theoretical and Applied Genetics. 2019:**132**(3):797–816.
1284 https://doi.org/10.1007/s00122-018-3252-x
1285 **Vert G, Grotz N, Dédaldéchamp F, Gaymard F, Guerinot ML, Briat JF, and Curie**
1286 **C**. CORRECTION: IRT1, an arabidopsis transporter essential for iron uptake
1287 from the soil and for plant growth. The Plant Cell. 2021:**33**(2):439–440.
1288 https://doi.org/10.1093/plcell/koaa033
1289 **Wickham H**. ggplot2: Elegant Graphics for Data Analysis. 2016.
1290 **Wu Y, Zhao Q, Gao L, Yu X-M, Fang P, Oliver DJ, and Xiang C-B**. Isolation and
1291 characterization of low-sulphur-tolerant mutants of Arabidopsis. Journal of
1292 Experimental Botany. 2010:**61**(12):3407–3422.
1293 https://doi.org/10.1093/jxb/erq161
1294 **Yoshimoto N, Takahashi H, Smith FW, Yamaya T, and Saito K**. Two distinct high-
1295 affinity sulfate transporters with different inducibilities mediate uptake of sulfate
1296 in *Arabidopsis* roots. The Plant Journal. 2002:**29**(4):465–473.
1297 https://doi.org/10.1046/j.0960-7412.2001.01231.x
1298 **Yoshiyama K, Conklin PA, Huefner ND, and Britt AB**. Suppressor of gamma
1299 response 1 (SOG1) encodes a putative transcription factor governing multiple
1300 responses to DNA damage. Proceedings of the National Academy of Sciences.
1301 2009:**106**(31):12843–12848. https://doi.org/10.1073/pnas.0810304106
1302 **Zahra N, Hafeez MB, Shaukat K, Wahid A, and Hasanuzzaman M**. Fe toxicity in
1303 plants: Impacts and remediation. Physiologia Plantarum.
1304 2021:**173**(1):ppl.13361. https://doi.org/10.1111/ppl.13361
1305 **Zandalinas SI and Mittler R**. Plant responses to multifactorial stress combination.
1306 New Phytologist. 2022:**234**(4):1161–1167. https://doi.org/10.1111/nph.18087
1307 **Zandalinas SI, Sengupta S, Fritschi FB, Azad RK, Nechushtai R, and Mittler R**.
1308 The impact of multifactorial stress combination on plant growth and survival.
1309 New Phytologist. 2021:**230**(3):1034–1048. https://doi.org/10.1111/nph.17232

1310 **Zhang C-J, Zhao B-C, Ge W-N, Zhang Y-F, Song Y, Sun D-Y, and Guo Y**. An
1311 Apoplastic H-Type Thioredoxin Is Involved in the Stress Response through
1312 Regulation of the Apoplastic Reactive Oxygen Species in Rice. Plant
1313 Physiology. 2011:**157**(4):1884–1899. https://doi.org/10.1104/pp.111.182808
1314 **Zhao B, Shao Z, Wang L, Zhang F, Chakravarty D, Zong W, Dong J, Song L, and**
1315 **Qiao H**. MYB44-ENAP1/2 restricts HDT4 to regulate drought tolerance in
1316 Arabidopsis. PLOS Genetics. 2022a:**18**(11):e1010473.
1317 https://doi.org/10.1371/journal.pgen.1010473
1318 **Zhao F-J, Tang Z, Song J-J, Huang X-Y, and Wang P**. Toxic metals and metalloids:
1319 Uptake, transport, detoxification, phytoremediation, and crop improvement for
1320 safer food. Molecular Plant. 2022b:**15**(1):27–44.
1321 https://doi.org/10.1016/j.molp.2021.09.016
1322

1323 **Author contributions**

1324 Research design: CH, VV and KG; Data acquisition: CH, DA, T Balliau, AO and MZ;
1325 Data processing: T Bonnot, CH, MT and JK; Data mining and visualization: T Bonnot;
1326 Data interpretation: T Bonnot, CH, MT, VV and KG; Writing – original draft: T Bonnot,
1327 CH, VV and KG; Manuscript review and editing: T Bonnot, CH, DA, JK, MT, T Bailliau,
1328 AO, MZ, VV and KG.
1329

1330 **Supplemental Table S1**. Arabidopsis genes identified in the same orthogroup
1331 (ORTHO05D000330) as *Psat0s2726g0040*, according to the Dicots PLAZA v.5
1332 database.

Gene ID	Description
AT1G49010	MYB-like transcription factor; ATMYBL, MYBS1
AT2G38090	Duplicated homeodomain-like superfamily protein
AT3G10580	Homeodomain-like superfamily protein
AT3G10585	Homeodomain-like superfamily protein
AT3G11280	Putative transcription factors interacting with the gene product of VHA-B1
AT4G09450	Duplicated homeodomain-like superfamily protein
AT5G01200	Duplicated homeodomain-like superfamily protein
AT5G04760	R-R-type MYB protein; DIV2, DIVARICATA2
AT5G05790	Duplicated homeodomain-like superfamily protein
AT5G08520	Duplicated homeodomain-like superfamily protein; MYBS2
AT5G58900	R-R-type MYB protein ; DIV1, DIVARICATA1

1333

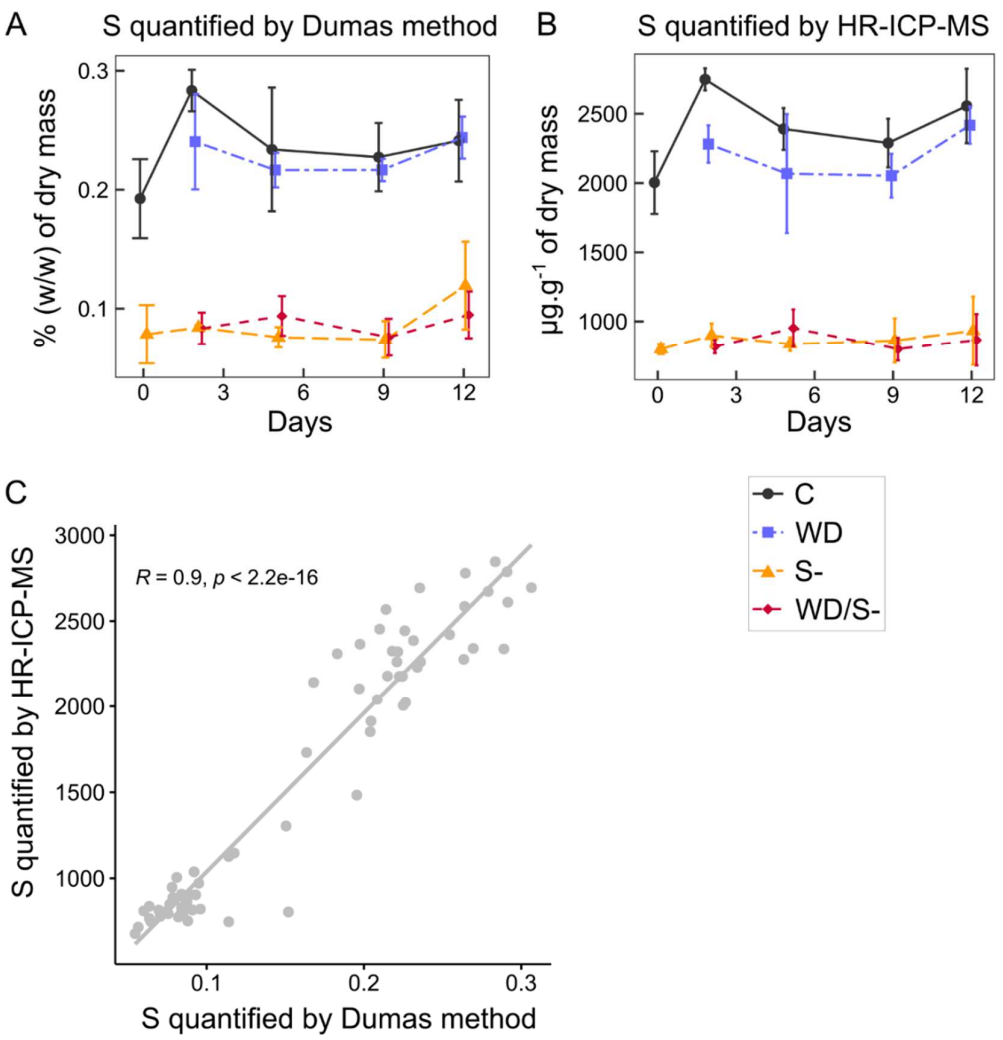

Supplemental Figure S1. Quantification of sulfur (S) in leaves: correlation between the two quantification methods. A, S percent measured using the Dumas method. B, S measured using high-resolution inductively coupled plasma mass spectrometry (HR ICP-MS). In A and B, data are means ± S.D of n = 4 replicates. C: control, WD: water deficit, S-: S deficiency. Note that day 12 corresponds to three days of rewatering in the WD and WD/S- conditions. C, Correlation between data obtained by HR ICP-MS (ionomics, B) and by the Dumas method (A). The correlation (Spearman) coefficient and P-value are indicated.

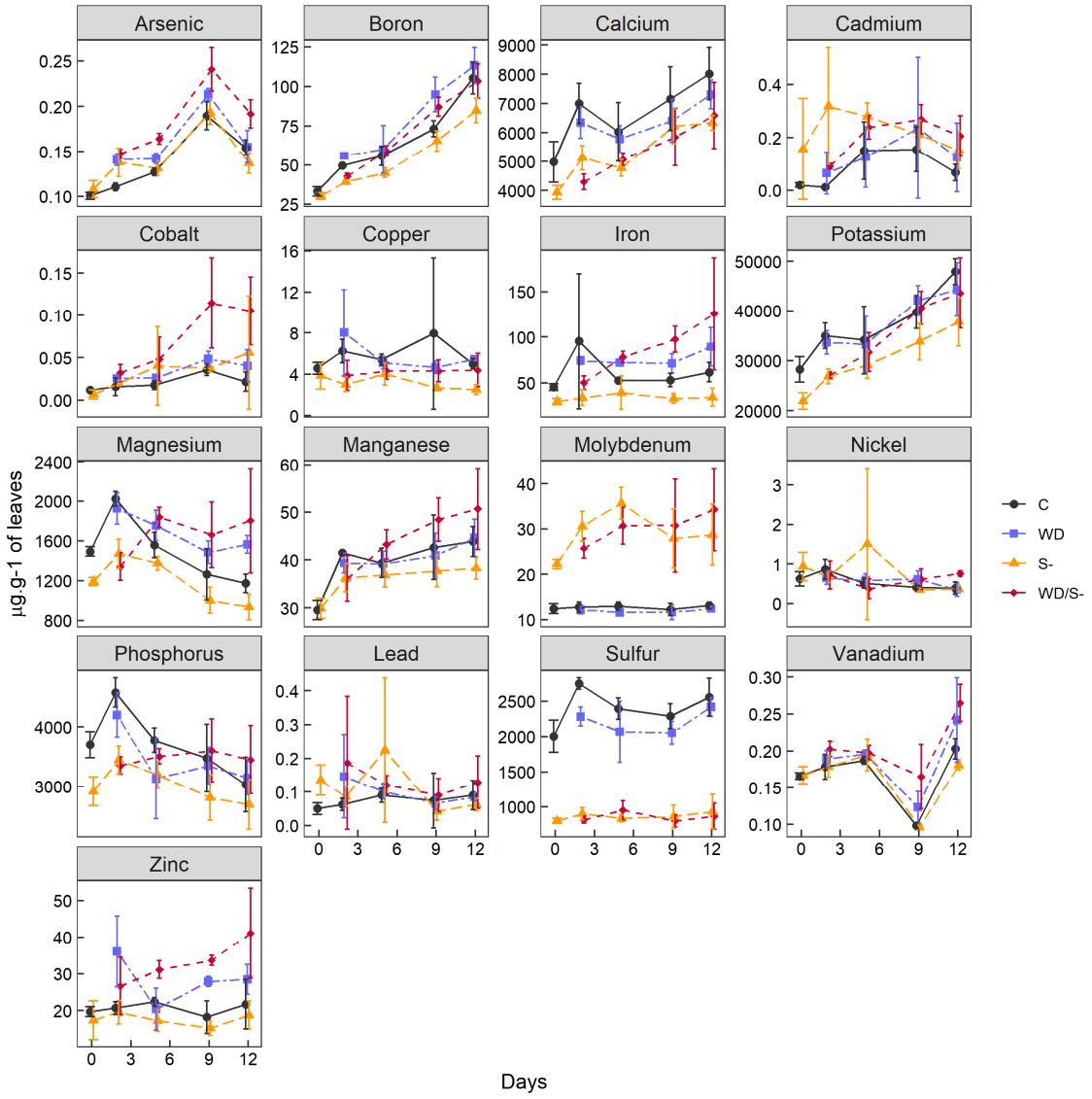

Supplemental Figure S2. Accumulation profiles of elements over time in leaves. Data are means ± S.D of *n* = 4 biological replicates. C: control, WD: water deficit, S-: Sulfur deficiency. Note that day 12 corresponds to three days of rewatering in the WD and WD/S- conditions.

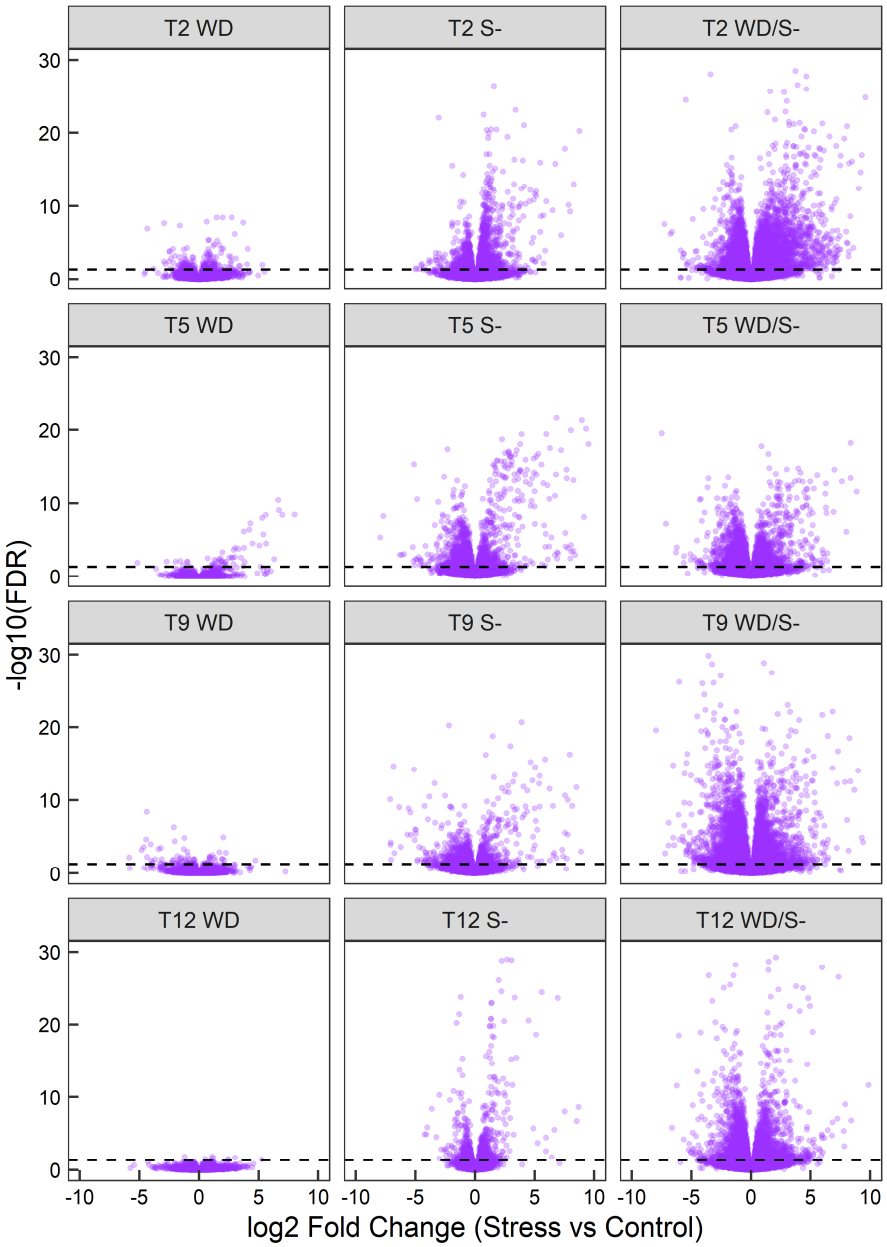

Supplemental Figure S3. Volcano plots representing statistical significance (-log10[FDR]) versus magnitude of change (Log_2 Fold Change) for mRNAs. WD: water deficit, S-: Sulfur deficiency. Note that T12 corresponds to three days of rewatering in the WD and WD/S- conditions.

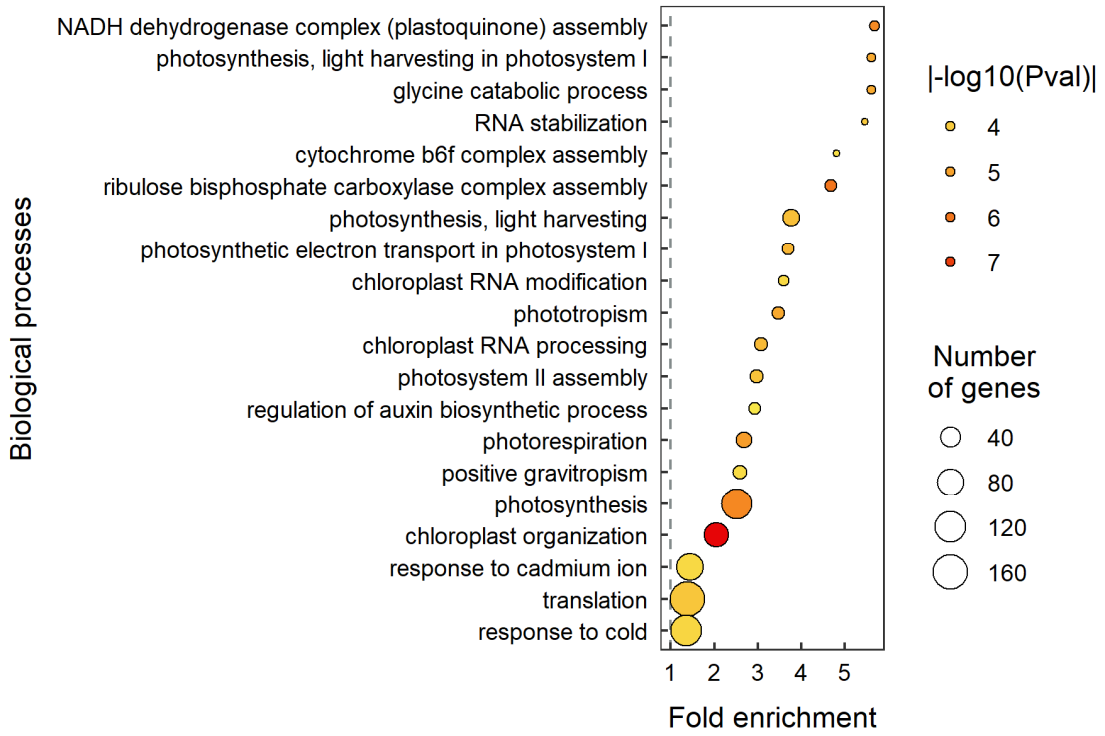

Supplemental Figure S4. Selected enriched biological processes in the list of genes with a specific or amplified down-regulation under WD/S- as compared to single stress conditions. The top 20 enriched GO terms (based on P-values) are represented. Results of the GO enrichment analysis are provided in Supplemental Data Set S5.

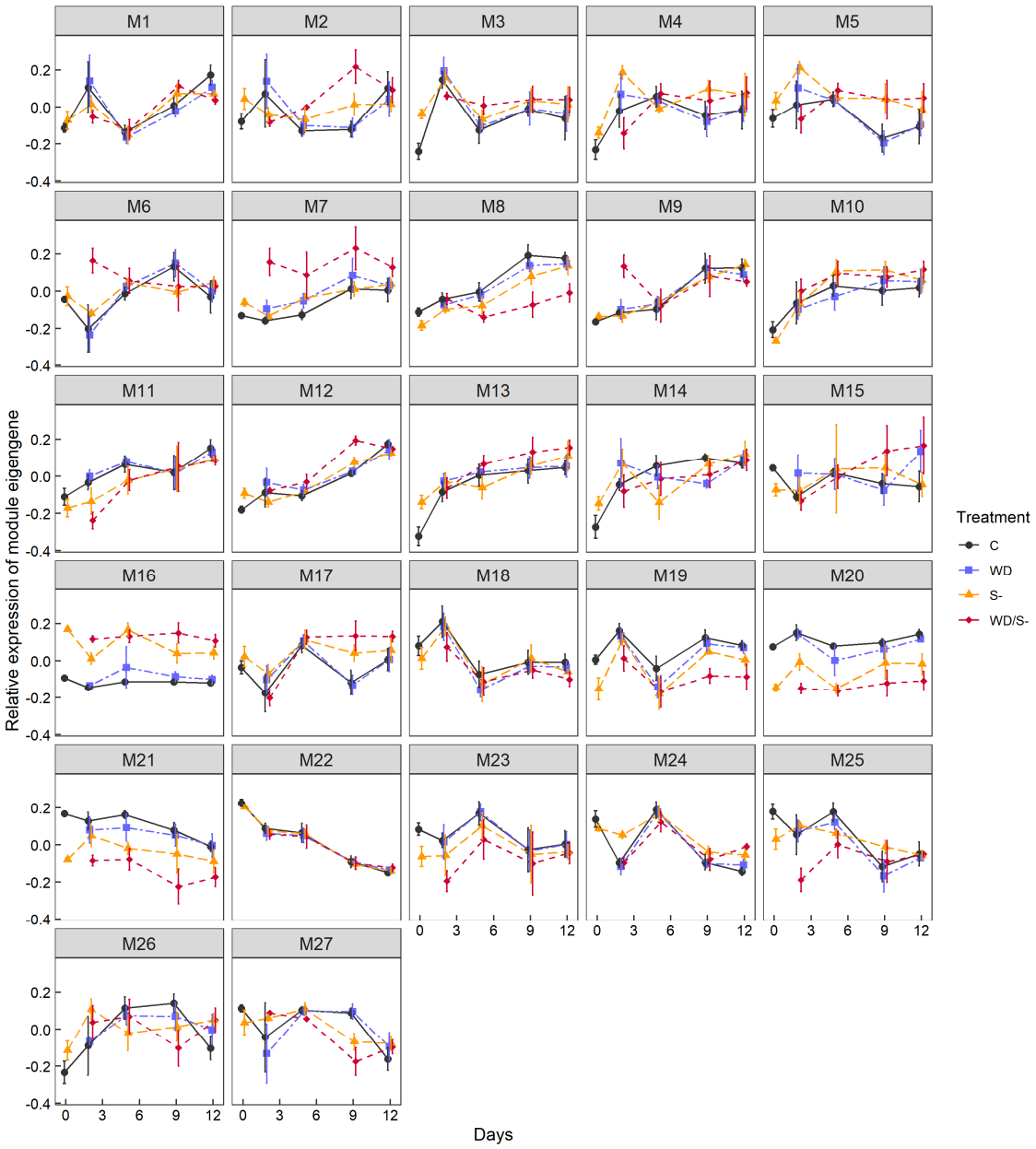

Supplemental Figure S5. Profiles of module eigengenes for modules identified in the co-expression network analysis, performed from transcriptomic data. Data are means ± S.D. for $n = 4$ replicates. C: control, WD: water deficit, S-: Sulfur deficiency. Note that day 12 corresponds to three days of rewatering in the WD and WD/S- conditions.

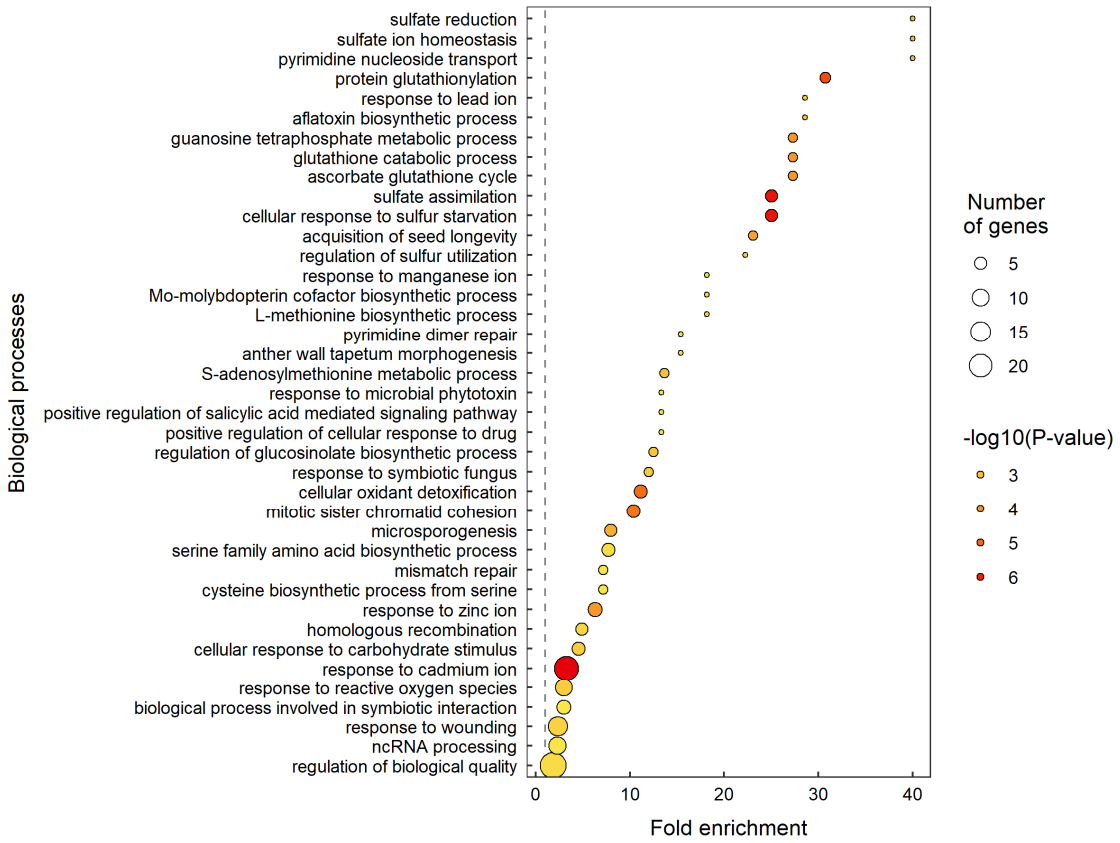

Supplemental Figure S6. Enriched biological processes in the list of 520 genes grouped in module M16. Results of the GO enrichment analysis for all modules are provided in Supplemental Data Set S5.

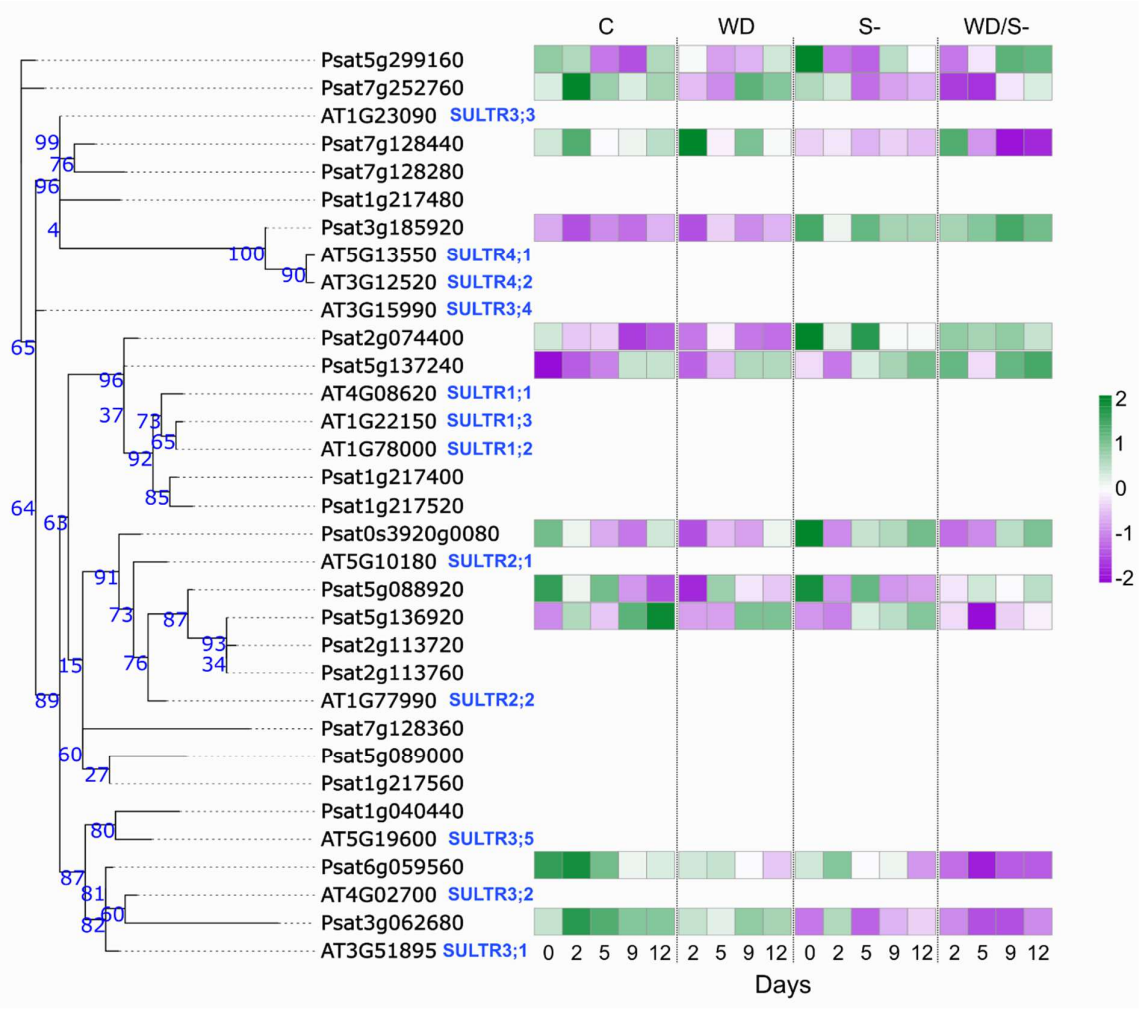

Supplemental Figure S7. Response to stress of sulfate transporters. Phylogenetic tree of sulfate transporters was built using the interactive phylogenetics module of the Dicots PLAZA v5 database (https://bioinformatics.psb.ugent.be/plaza/). Confidence numbers are indicated on the tree branches and provide insights into the reliability of the inferred relationships between sequences. Heatmap represents expression levels of sulfate transporters over time and under control and stress conditions. Data are scaled and are means of *n* = 4 replicates. Only genes identified as expressed in the experiment and selected for the weighted gene co-expression network analysis are represented. Purple and green colors indicate low and high expression levels, respectively. C: control, WD: water deficit, S-: Sulfur deficiency. Note that day 12 corresponds to three days of rewatering in the WD and WD/S- conditions.

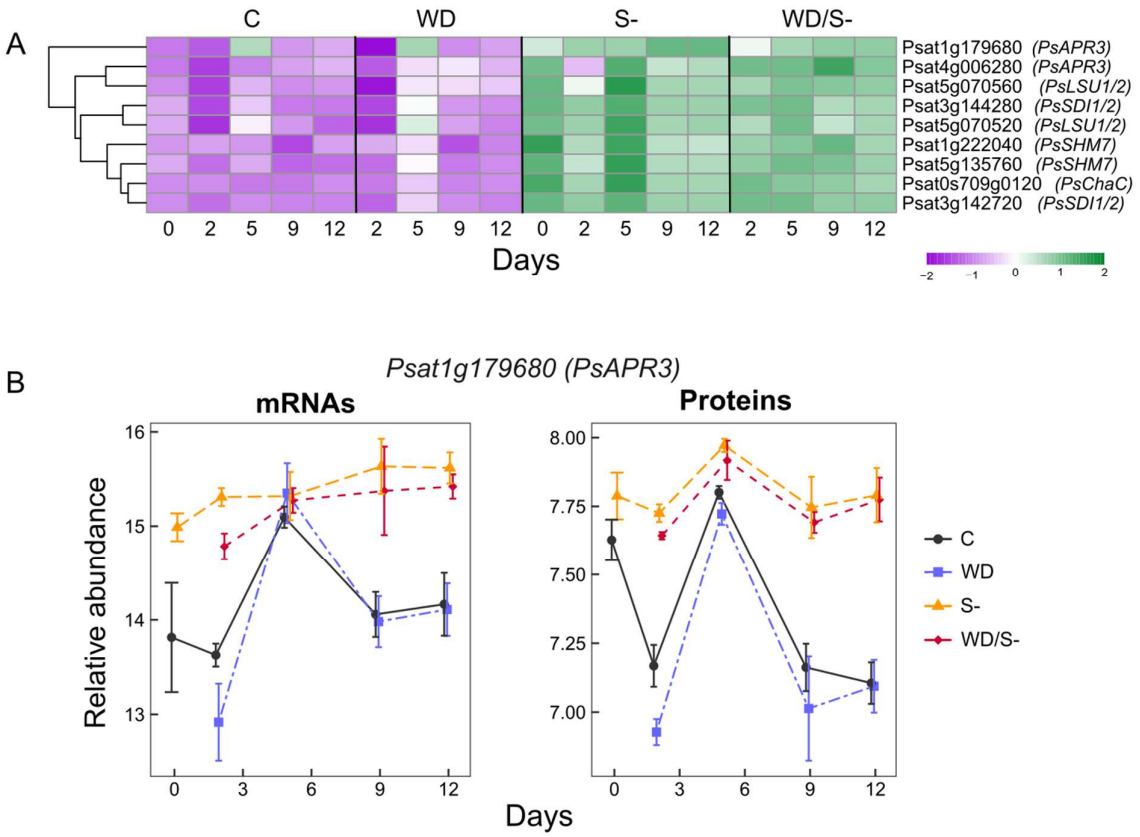

Supplemental Figure S8. Response to stress of OAS cluster genes. A, Heatmap representing expression levels of OAS cluster genes over time and under control and stress conditions. Best homologous genes of Arabidopsis OAS cluster genes were identified using reciprocal BLASTP. Data are scaled and are means of $n = 4$ replicates. Only genes identified as expressed in the experiment and selected for the weighted gene co-expression network analysis are represented. Purple and green colors indicate low and high expression levels, respectively. C, Expression profile of *Psat1g179680*, which was analyzed at both transcriptome and proteome levels (means ± S.D, $n = 4$ replicates). C: control, WD: water deficit, S-: Sulfur deficiency. Note that day 12 corresponds to three days of rewatering in the WD and WD/S- conditions.

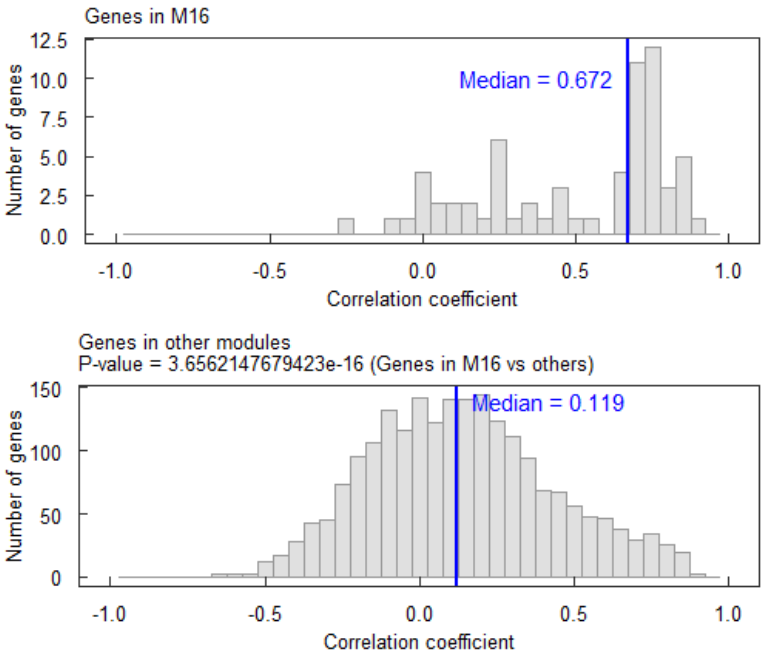

Supplemental Figure S9. Distribution of correlation (Protein vs mRNA, Spearman correlation) coefficients within M16 and other modules. Vertical blue lines indicate medians. The P-value was calculated by comparing correlation coefficients within M16 vs other modules, using a Wilcoxon signed-rank test.

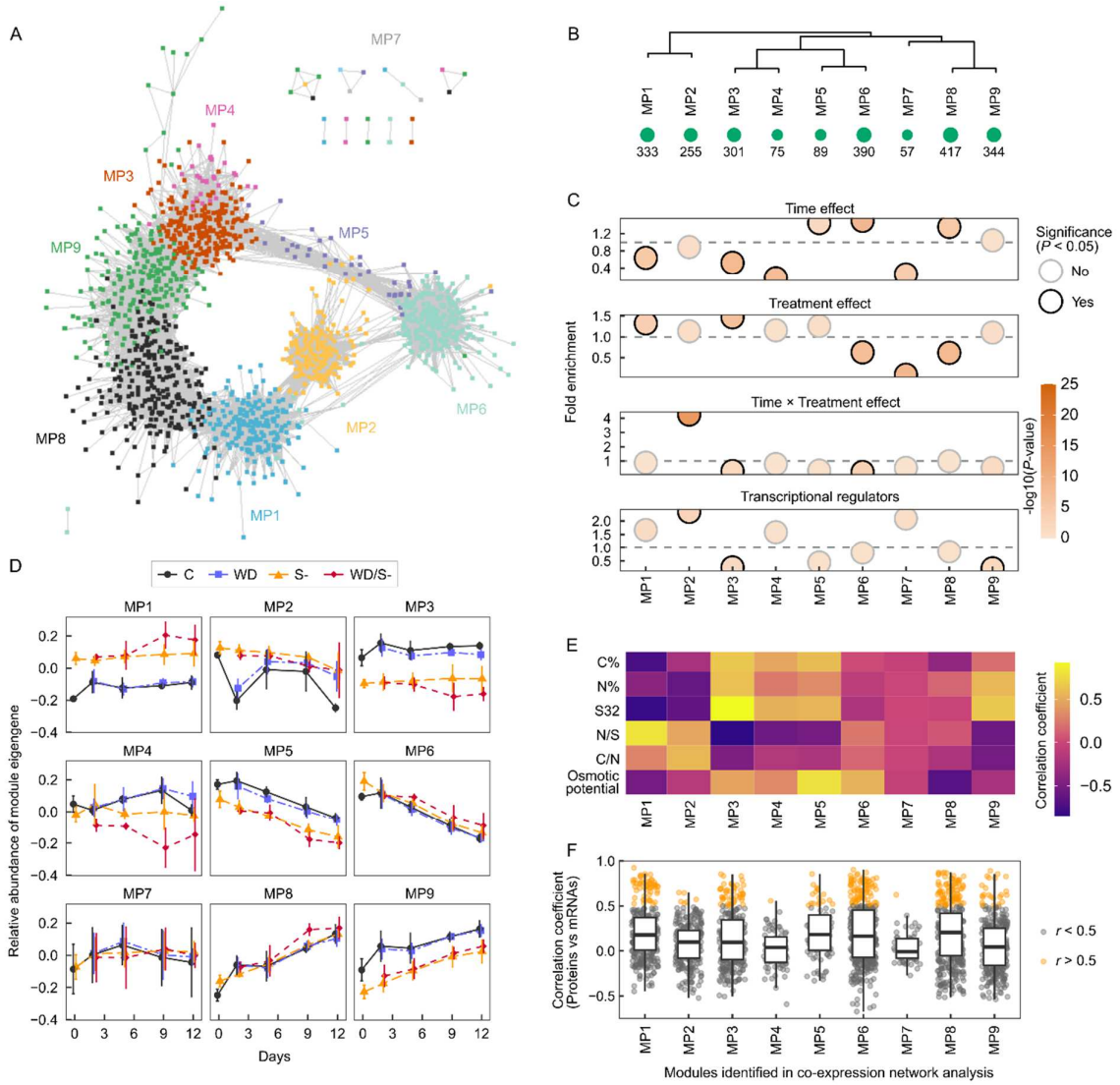

Supplemental Figure S10. Co-accumulation network of proteins reveals modules with distinct patterns of response to stress. A, Co-accumulation network generated with WGCNA and visualized in Cytoscape using a Prefuse Force Directed layout, with an edge threshold cutoff of weight > 0.10. This network was built from proteomics data. Nodes are colored according to their module membership. B, Clustering of module eigengenes. The module eigengene is defined as the first principal component of a given module (Langfelder and Horvath, 2008). Below module names, number of proteins assigned to each individual module are indicated and are represented as bubble plots. C, Bubble plots representing enrichment of specific groups of proteins within each individual module. Fold enrichment < 1 and > 1 correspond to an under- and over-representation in the module, respectively. Proteins with a time, treatment and/or time × treatment interaction effects were identified in Fig. 3A. Transcriptional

1418 regulators were identified using the PlantTFCat tool (see methods). D, Profiles of
1419 module eigengenes (means ± S.D, n = 4 replicates). E, Heatmap representing the
1420 correlation (Spearman) between trait data (elements and physiological parameters)
1421 and module eigengenes. F, Boxplots showing the distribution by module of correlation
1422 coefficients for the comparison protein vs mRNA. Dots represent individual genes.
1423 Genes with a correlation > 0.5 (Protein vs mRNA) are highlighted in orange.
1424 Boundaries of the boxes represent the 25th and 75th percentiles, and horizontal lines
1425 within boxes represent medians. C: control, WD: water deficit, S-: Sulfur deficiency.
1426 Note that day 12 corresponds to three days of rewatering in the WD and WD/S-
1427 conditions.

1428

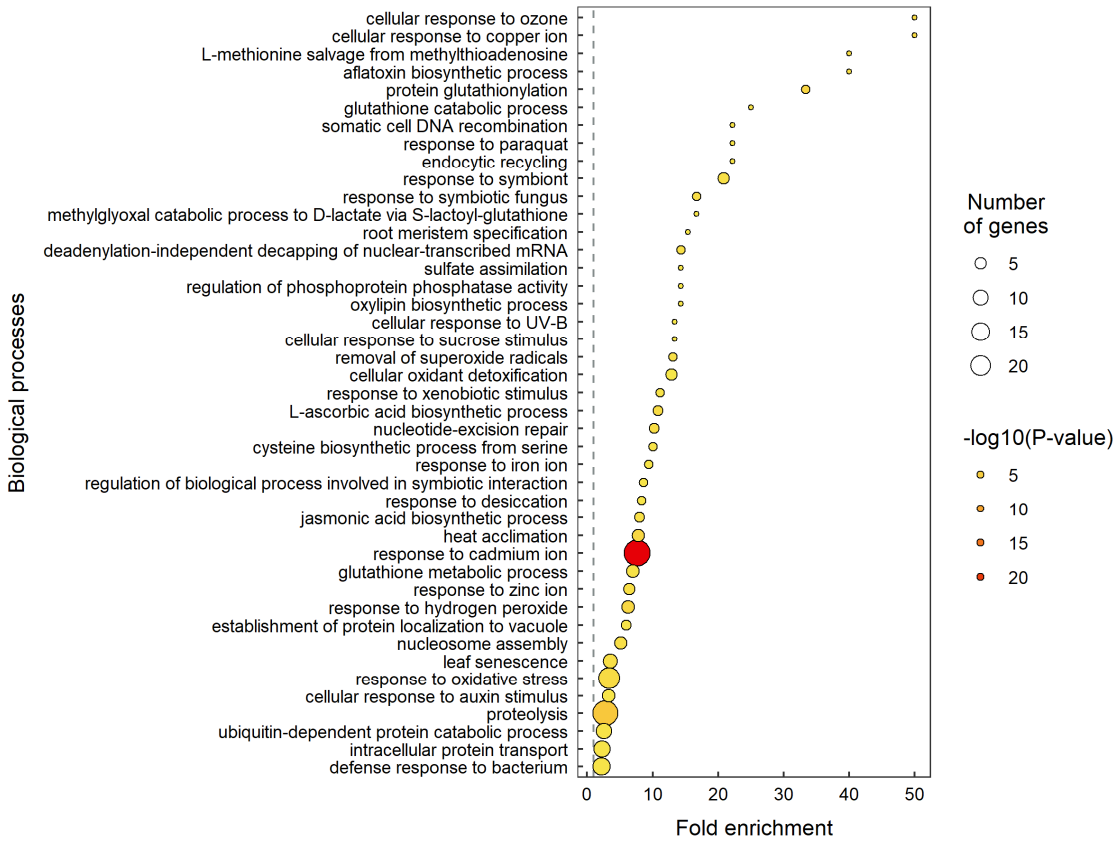

Supplemental Figure S11. Enriched biological processes in the list of 333 proteins grouped in module MP1. Results of the GO enrichment analysis for all modules are provided in Supplemental Data Set S5.

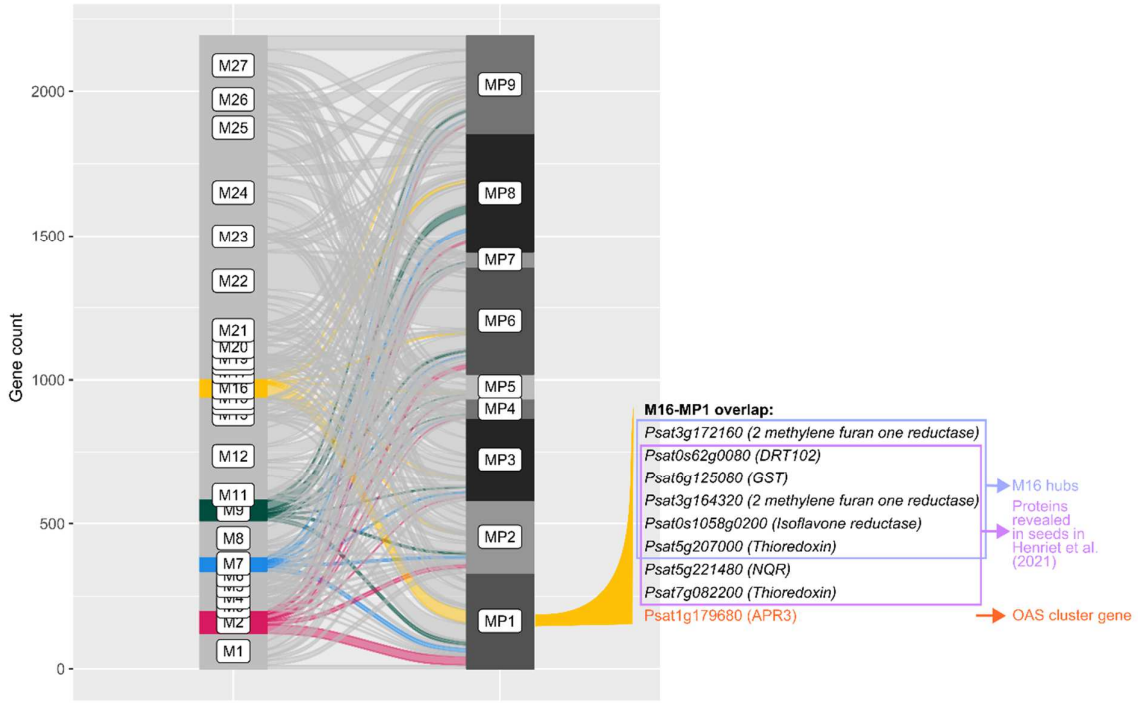

Supplemental Figure S12. Overlap between co-expression modules (transcriptomics data, left) and co-accumulation modules (proteomics data, right). Only genes that were analyzed at both the transcriptome and proteome levels are represented. Module M16 and modules M2/M7/M9, presented in Figures 5 and 6, respectively, are highlighted. Selected genes from the overlap between modules M16 and MP1 are indicated.

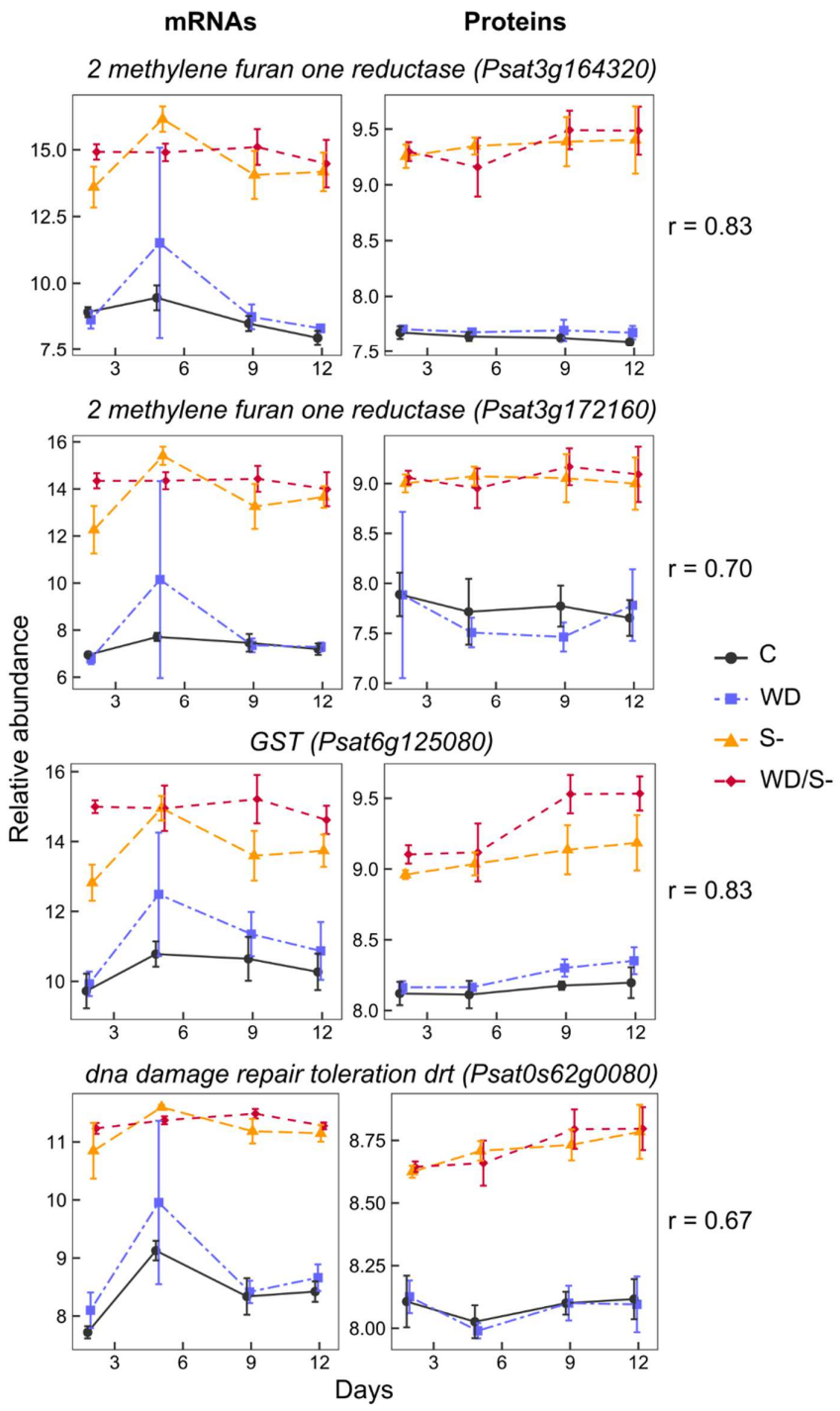

1440

1441 **Supplemental Figure S13**. Expression profiles (mRNAs and proteins) of selected
1442 hubs in module M16 (means ± S.D, *n* = 4 replicates). Correlation (Spearman)
1443 coefficients for the comparison protein vs mRNA are indicated next to the plots. C:
1444 control, WD: water deficit, S-: Sulfur deficiency. Note that day 12 corresponds to three
1445 days of rewatering in the WD and WD/S- conditions.

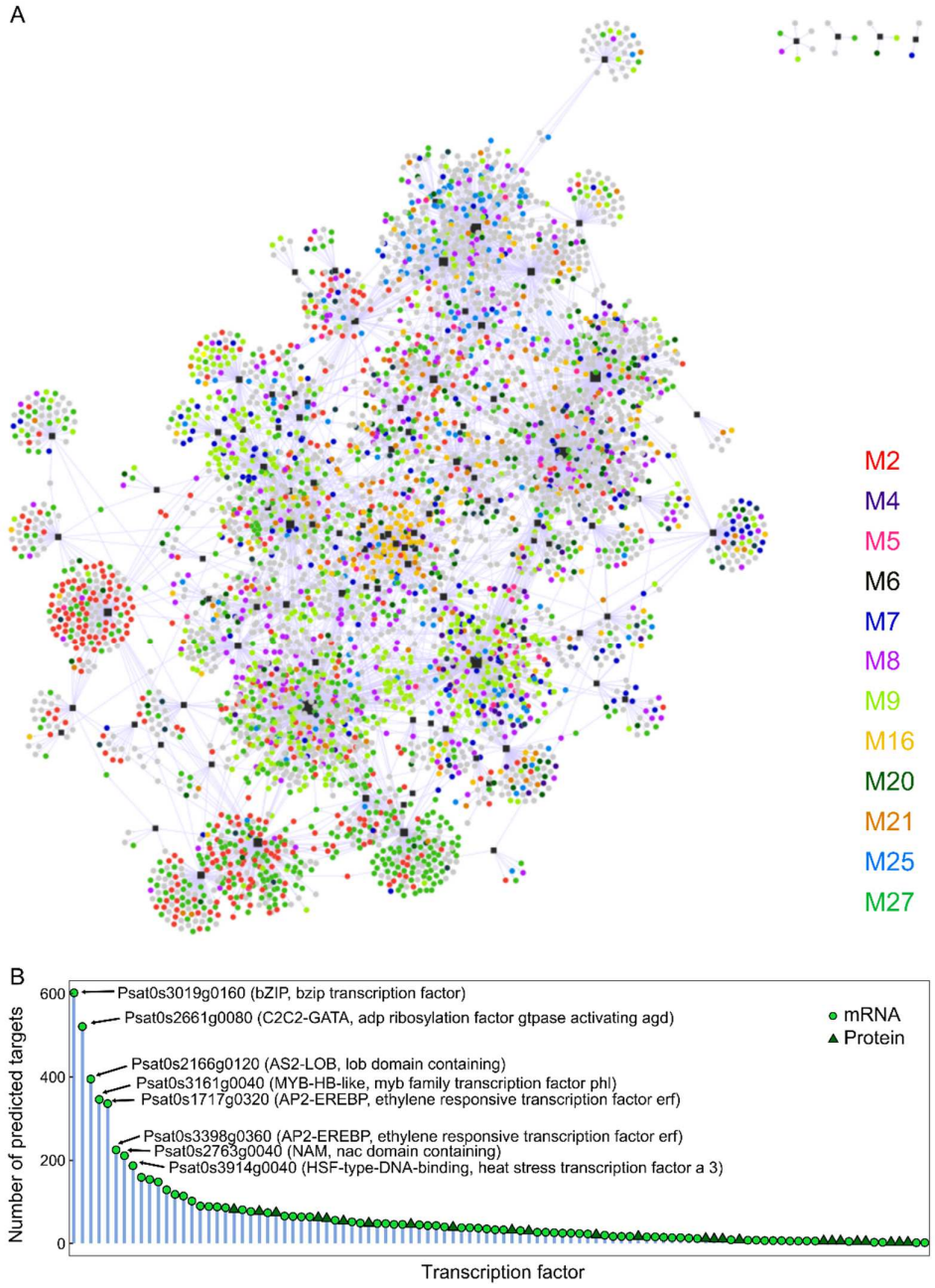

Supplemental Figure S14. Prediction of regulatory connections between TFs and their target genes. A, Gene regulatory network. Edges correspond to regulatory connections predicted with the tool dynGENIE3, and are oriented from regulators to target genes. Regulators are TFs and correspond to proteins or mRNAs (when data for the transcription factor was not available at the proteome level). Targets correspond to mRNAs. Regulators are colored in black and targets are colored according to their module membership in the co-expression network presented in Figure 4. B, Regulators ranked by their number of predicted targets.

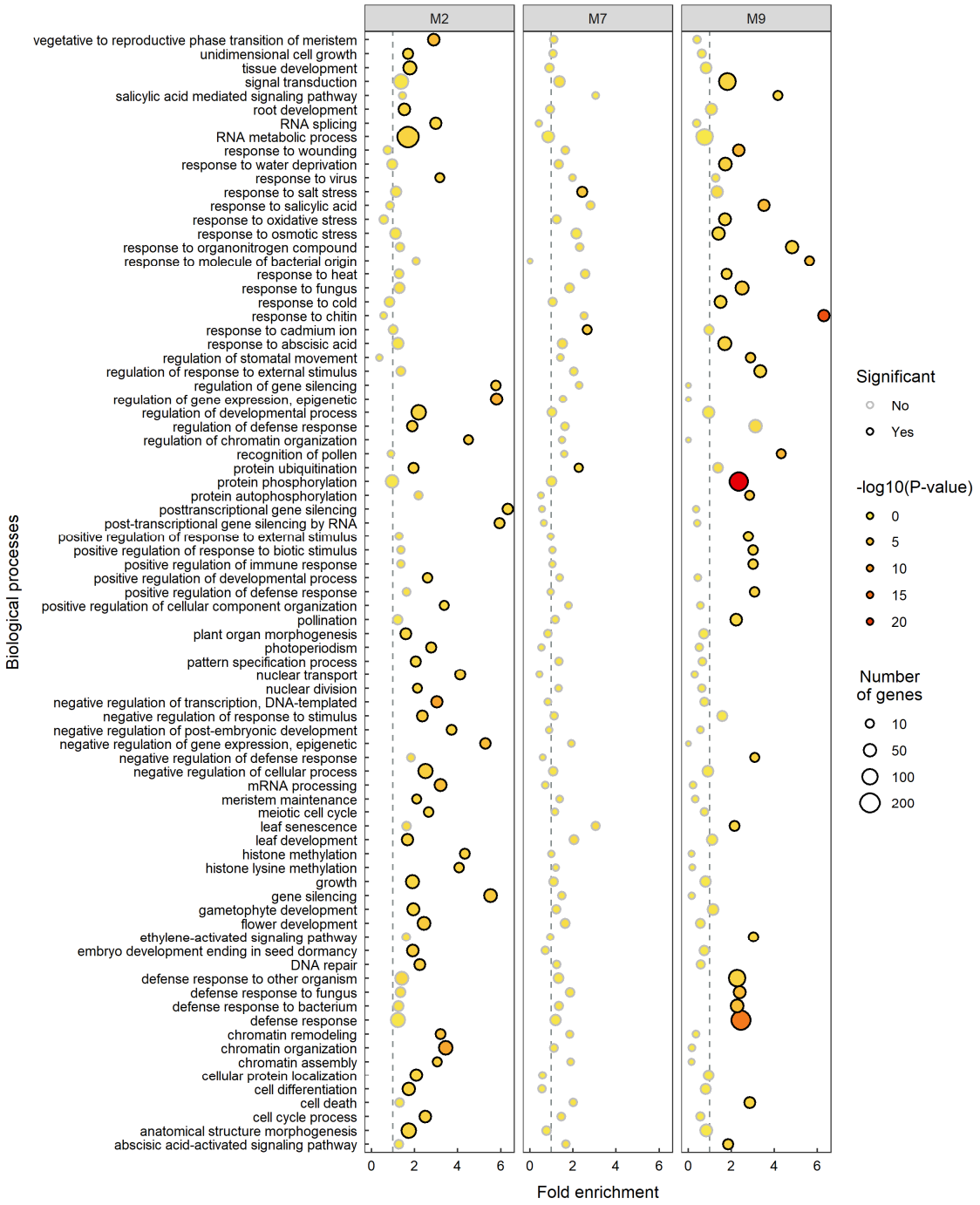

Supplemental Figure S15. Selected enriched biological processes in modules M2 (1368 genes), M7 (478 genes) and M9 (1578 genes). Selected processes were significantly over-represented in any of the three modules, with a minimum of 15 genes. Results of the GO enrichment analysis are provided in Supplemental Data Set S5.

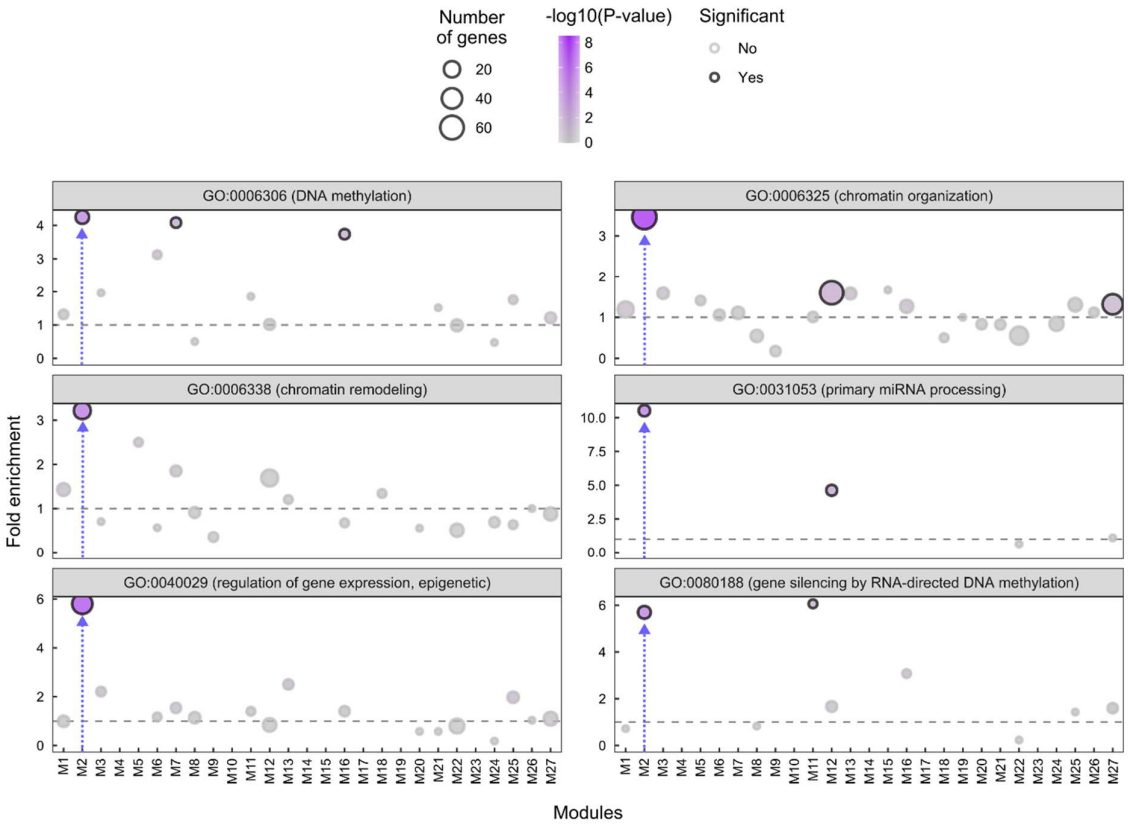

Supplemental Figure S16. Enrichment of biological processes related to epigenetic mechanisms in co-expression modules. Vertical blue arrows indicate enrichment in module M2. Results of the GO enrichment analysis are provided in Supplemental Data Set S5.

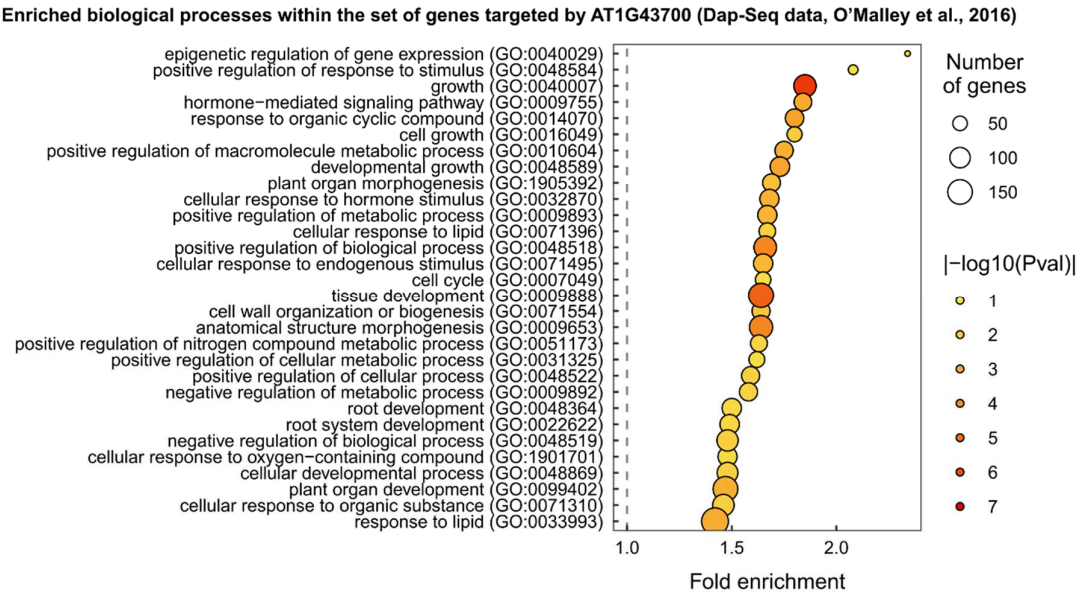

Supplemental Figure S17. Enriched biological processes within the list of genes targeted by AT1G43700, identified as homologous to the regulator R1. Only the top 30 enriched processes (based on fold enrichment values) are represented. Targets of AT1G43700 were identified using the DAP-Seq data produced by O'Malley et al. (2016).